PERGAMON

Deep-Sea Research I 46 (1999) 1861–1893

DEEP-SEA RESEARCH
PART I

Global distribution of the ^{230}Th flux to ocean sediments constrained by GCM modelling

Gideon M. Henderson[a,*], Christoph Heinze[b], Robert F. Anderson[a], Arne M.E. Winguth[c]

[a]*Lamont-Doherty Earth Observatory of Columbia University, Route 9W, Palisades, NY 10964, USA*
[b]*Max-Planck-Institut fur Meteorologie, Bundesstrasse 55, D-20146 Hamburg, Germany*
[c]*Department of Geophysical Sciences, University of Chicago, IL 60637, USA*

Received 23 February 1998; received in revised form 15 September 1998; accepted 28 December 1998

Abstract

We have introduced a simple particle field into an existing and well-documented ocean general circulation model. This enables us to investigate the advection and scavenging of particle-reactive species within the water column. As a first use of this model, we have assessed the advection and flux to sediment of ^{230}Th, a nuclide with a well understood marine chemistry that exhibits extreme particle reactivity. The flux to sediment of this nuclide is of interest as it is widely assumed to be related only to water depth, and therefore to act as a constant-flux indicator for marine sediments. By assuming an average settling velocity for marine particles of 3 m/d, in good agreement with observational constraints, the model generates a particle field close to that observed. Thorium-230 is scavenged onto this particle field reversibly according to Kd values constrained by observations and incorporating a particle-concentration effect. This scavenging gives a good fit to the ≈ 900 literature water-column measurements of ^{230}Th suggesting that the model is advecting and removing ^{230}Th realistically. An exception to this is the Weddell Sea, where the model has too little ice cover and too much lateral mixing, which prevents it from duplicating the observed high ^{230}Th values. The model confirms that significant advection of ^{230}Th occurs and duplicates the low ^{230}Th values seen deep in the North Atlantic due to the advection of low-^{230}Th surface waters to depth. Model-derived maps of the ^{230}Th flux to the sediment indicate that $\approx 70\%$ of the ocean floor receives a ^{230}Th flux within 30% of that expected from production. In extremely non-productive regions, the flux can fall to as low as 0.4 times that expected for in situ scavenging, while highly productive regions have fluxes up to 1.6 times that expected. An additional model run using glacial circulation fields suggests that glacial ^{230}Th fluxes are similar to those in the Holocene except in regions close to

* Corresponding author. Department of Earth Sciences, Oxford University, Parks Road, Oxford, England. Fax: + 44(0)1865272072.

E-mail addresses: gideonh@earth.ox.ac.uk (G.M. Henderson), heinze@dkrz.de (C. Heinze), boba@ldeo.columbia.edu (R.F. Anderson), winguth@starbuck.uchicago.edu (A.M.E. Winguth)

0967-0637/99/$ - see front matter
PII: S0967-0637(99)00030-8

sea ice. This is particularly true of the North Atlantic, where appreciably more scavenging occurs in the glacial run due to advection of ^{230}Th from the ice-covered Arctic, and because of reduced North Atlantic Deep Water (NADW) formation. These ice-related effects mean that the area of ocean floor with ^{230}Th fluxes within 30% of production falls to $\approx 60\%$ for the glacial. The Holocene and Glacial flux maps allow an assessment of the accuracy of ^{230}Th-derived sedimentation rates for existing and future studies.

Keywords: ^{230}Th; Scavenging; Ocean modelling; Particles; Paleoceanography

1. Introduction

Measuring the concentration of a chemical or mineral constituent of marine sediment is generally straightforward. But converting this concentration into the flux of that constituent into the sediment is more difficult. One way of making this conversion is by dating two horizons in the sediment and calculating the flux between them, but this approach assumes uniform flux between the two dated horizons. A potentially more powerful approach is to use a chemical species that has a constant input to the sediment, so that the concentration of the constituent of interest, relative to that of the constant-flux indicator, provides an "instantaneous" measure of the flux of the constituent. One such constant-flux indicator is ^{230}Th.

Thorium-230 is produced continuously in seawater from the radioactive decay of uranium but occurs at very low concentrations in seawater (Bacon and Anderson, 1982; Moore, 1981; Nozaki et al., 1981). This is due to its extreme particle-reactive nature such that, almost as soon as it is produced, it adheres to particles suspended in sea water and is removed to the seafloor when these particles sink (a process termed "scavenging"). The temporally and spatially uniform production of ^{230}Th, coupled with its rapid removal to marine sediment, means that the expected flux to the sediment can be readily calculated for any water depth and this flux used to calculate the flux of other sediment constituents. Thorium-230 has been widely used in this way to elucidate past fluxes of mineral and chemical constituents into marine sediments (e.g. Bacon and Rosholt, 1982; Francois et al., 1990; Suman and Bacon, 1989).

The accuracy of the ^{230}Th constant-flux technique, however, is limited by the assumption that ^{230}Th is removed from seawater as soon as it is formed without any prior advection. That this assumption is not completely robust is demonstrated by the fact that ^{230}Th exists at all as a dissolved species in seawater. The extent of deviation from the ideal zero-advection case has previously been tested through the use of sediment-trap studies (Anderson et al., 1983a,b; Bacon et al., 1985; Colley et al., 1995; Taguchi et al., 1989) and, more recently, against other flux indicators in Pleistocene sediments (Marcantonio et al., 1995; Thomson et al., 1997). Sediment-trap studies have demonstrated that some deviations from the zero-advection case exist. But these studies suffer from the common problem of failing to achieve 100% recovery. In addition, both the above approaches for assessing ^{230}Th scavenging allow measurements only at individual points, not over geographical areas. Although these studies

have provided useful indications of the limits of the ^{230}Th constant-flux technique, they fall short of providing a global assessment of the spatial and temporal variability of the ^{230}Th flux to marine sediments.

Several recent studies of water-column ^{230}Th concentrations have clearly demonstrated that advection of ^{230}Th must occur in the oceans. The best example is in the North Atlantic region where low-^{230}Th surface waters are being advected to depth by North Atlantic Deep Water (NADW) formation (Moran et al., 1997,1995; Vogler et al., 1998). Similar advection of low-^{230}Th waters has been proposed for the Nansen basin in the Arctic (Cochran et al., 1995) and of high-^{230}Th waters for the South Atlantic (Rutgers van der Loeff and Berger, 1993). If such advection of ^{230}Th occurs, ^{230}Th fluxes cannot be expected to be completely constant, and an assessment of the variability of the flux around the globe is needed.

The geochemistry of thorium in seawater is well enough understood that we are able to approach this problem by the application of global modelling. In this study, we have modified a well documented General Circulation Model (GCM) of the oceans to accurately handle particles and particle-reactive chemical species. This model is tested against existing water-column measurements of ^{230}Th and is then used to derive estimates of advection of ^{230}Th and of the spatial variability of the flux of ^{230}Th to marine sediments. We present results for both the pre-industrial Holocene, and a more tentative estimate for the last glacial maximum.

2. Marine chemistry of thorium and ^{230}Th observations

Thorium-230 in seawater was first measured in the particulate phase by filtration (Krishnaswami et al., 1976; Krishnaswami et al., 1981) and then in total seawater (Moore, 1981; Nozaki et al., 1981). These studies showed a linear increase in ^{230}Th concentration with water depth, and total concentrations ≈ 10 times the particulate-only concentrations. Numerous other studies have since measured ^{230}Th in the water column (Anderson et al., 1983a,b; Bacon and Anderson, 1982; Bacon et al., 1989; Cochran et al., 1995,1987; Colley et al., 1995; Guo et al., 1995; Hoff et al., in press; Huh and Beasley, 1987; Luo et al., 1995; Mangini and Key, 1983; Moran et al., 1997,1995; Nozaki and Horibe, 1983; Nozaki and Nakanishi, 1985; Nozaki and Yamada, 1987; Nozaki and Yang, 1987; Nozaki et al., 1987; Roy-Barman et al., 1996; Rutgers van der Loeff and Berger, 1993; Scholten et al., 1995; Vogler et al., 1998, in press; Walter et al., 1997).

The basic features of the ^{230}Th profile in seawater are best explained by a reversible scavenging model (Bacon and Anderson, 1982; Nozaki et al., 1987) in which ^{230}Th adheres to particles in the upper water column but continues to exchange with seawater as the particles settle. From laboratory (Moore and Hunter, 1985) and field (Bacon and Anderson, 1982) studies of shorter-lived Th isotopes (e.g. ^{234}Th), this exchange has been shown to occur relatively quickly so that, on time-scales of months or longer, particulate and dissolved Th are in equilibrium. This equilibrium condition can be described by the use of a distribution coefficient, Kd, defined as the concentration of ^{230}Th per mass of particles divided by the concentration of ^{230}Th per mass of

water. The extreme particle affinity of ^{230}Th is demonstrated by Kd values greater than 10^5.

In areas where particle concentrations are high, such as productive areas and coastal margins, Kd values have been shown to be systematically lower than in areas with lower particle concentrations (Guo et al., 1995; Honeyman et al., 1988). This behaviour has been ascribed to an increase in colloid concentration accompanying increased particulate concentrations, which keeps some ^{230}Th on small particles that pass through filters upon sampling (Santschi and Honeyman, 1991). It may also be related to the tendency of particles to stick together as they become more common and thus to offer less surface area for Th scavenging. The natural variation in Kd with particle concentrations is shown in Fig. 1.

Most early studies of particle-reactive elements assumed that they adhered approximately equally to all particles types (carbonate, opal, particulate-organic-carbon, Fe–Mn oxyhydroxides, and terrigenous). More recently, several studies have demonstrated the unsurprising result that many elements show differing affinities for each particle type. For instance, ^{231}Pa is known to adhere more readily to Mn oxides (Anderson et al., 1983a) and to opal (Lao et al., 1993; Walter et al., 1997). Such differential affinities have not, to date, been recognised for Th, although they have been looked for in at least one study (Yu, 1994). This may simply reflect the shorter residence time of Th, making any differential scavenging difficult to resolve. But in the absence of any evidence to the contrary we are forced here to consider that Th is scavenged by all particle types equally.

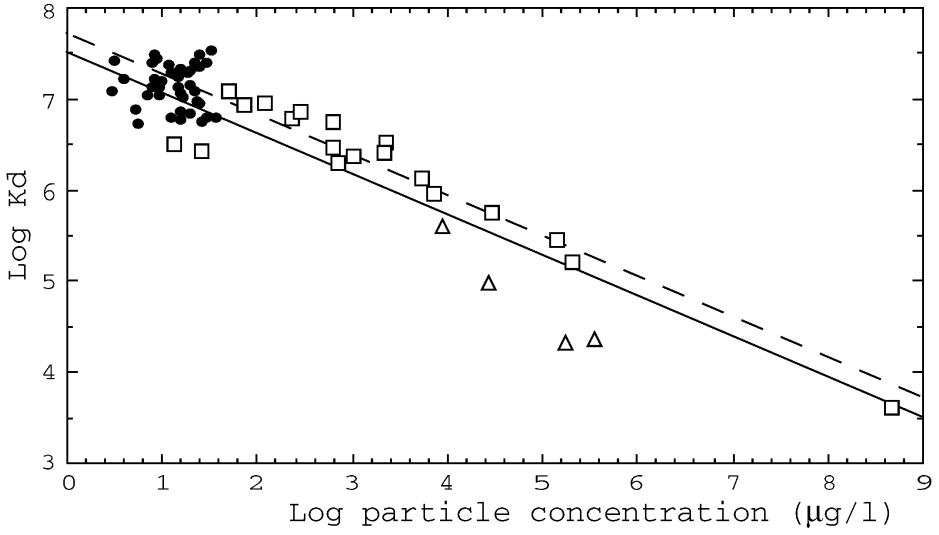

Fig. 1. Co-variation of observed Th Kd values with particle concentration. Open squares are marine ^{234}Th data from the compilation of Honeyman et al., 1988; open triangles are continental shelf ^{234}Th data from McKee et al. (1986), and filled circles are compiled from Bacon and Anderson, 1982; Bacon et al. (1989); Cochran et al. (1987); and Nozaki et al. (1987), and are open-marine ^{230}Th values. The dashed line is the best fit to the ^{234}Th data after Honeyman et al. (1998) and the solid line is the relationship used in this study.

Many particle-reactive elements exhibit a phenomenon termed "boundary scavenging," in which they are more heavily scavenged around the margins of the ocean basins than in the open ocean. This behaviour is apparently caused by several processes, including higher detrital particle fluxes, greater sediment mixing, and a strong affinity of some elements to Fe–Mn oxyhydroxides, which are more common in shelf and coastal environments. Boundary scavenging behaviour is exhibited by ^{230}Th (Anderson et al., 1983a,1994; Lao et al., 1993) but is not so marked as for other elements. This reflects the shorter residence time of Th, which provides less time for Th to be advected to the boundaries before scavenging. But it also appears to be a feature of the chemistry of Th. Elements that exhibit boundary scavenging generally show depletion in bottom water, close to the sediment–water interface. But ^{230}Th scavenging at the sediment–water interface has been observed only in extreme cases (Bacon and Anderson, 1982), and ^{234}Th does not exhibit bottom scavenging except in regions with a pronounced nepheloid layer (Bacon and Rutgers van der Loeff, 1989). These effects mean that ^{230}Th boundary scavenging is only in evidence close to shore. For instance ^{230}Th is scavenged in an open ocean fashion as close as 200 km from the coast in the NE Pacific (Lao et al., 1993). Boundary scavenging is not explicitly incorporated into the model presented in this paper. The scale at which it occurs is too fine to be well mimicked by the resolution of the model, and our primary interest in this study is the open-ocean advection and scavenging of ^{230}Th rather than near-shore processes.

For the purposes of this study, we have collated all existing water-column observations of ^{230}Th concentrations. After the early work conducted at single sites, there have been a number of more regional studies featuring several profiles in the Arctic ocean, the South Atlantic, the equatorial Pacific, and around Japan. Outside of these areas, and the North Atlantic, data coverage is sparse (see Fig. 2), but at the time of conducting this study a total of 341 dissolved ^{230}Th, 240 particulate ^{230}Th, and 347 total ^{230}Th measurements had been made with which to compare our modelling results. This data-collation is available at http://www.earth.ox.ac.uk/~gideonh/public.html.

Measurement of the very low ^{230}Th concentrations seen in seawater are still not routine and require large samples and low blanks. This difficulty yields typical uncertainty on the measured data in the order of 5–10%. Few inter-laboratory comparisons of seawater-^{230}Th measurements exist, so this may introduce additional error. Thus, there may be an uncertainty of some tens of percent in the use of any individual ^{230}Th measurement as an estimate of the annual mean value at a particular site. The data set is of a sufficient size, however, that general patterns of ^{230}Th concentrations must be robust.

To assess the success of the model at duplicating observations, we follow two approaches. First, we average all observed profiles for dissolved, particulate and total ^{230}Th to derive composite ^{230}Th depth profiles and compare these average profiles with average model profiles compiled in the same way from model output at the same locations. Second, we have selected seven of the individual sites where ^{230}Th observations exist as representative of global spatial variability, and we compare these sites with model values at the same points. The locations of these seven sites are indicated in Fig. 2 and are chosen as they are situated in the open ocean and have data covering a wide depth range. The ^{230}Th profiles at these seven sites are plotted in Fig. 3.

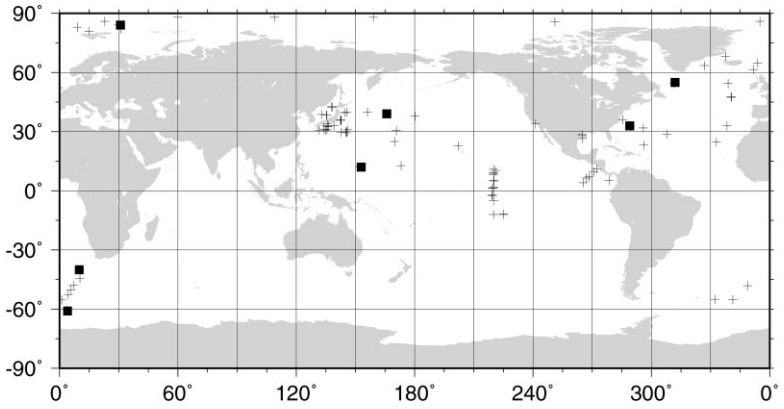

Fig. 2. Distribution of literature measurements of water-column ^{230}Th used in this study (Anderson et al., 1983a Anderson et al., 1983b; Bacon and Anderson, 1982; Bacon et al., 1989; Cochran et al., 1995,1987; Colley et al., 1995; Guo et al., 1995; Hoff et al., in press; Huh and Beasley, 1987; Luo et al., 1995; Mangini and Key, 1983; Moran et al., 1997 Moran et al., 1995; Nozaki and Horibe, 1983; Nozaki and Nakanishi, 1985; Nozaki and Yamada, 1987; Nozaki and Yang, 1987; Nozaki et al., 1987; Roy-Barman et al., 1996; Rutgers van der Loeff and Berger, 1993; Scholten et al., 1995; Vogler et al., in press, Vogler et al., 1998). The seven stations discussed in more detail in this paper are shown as filled squares (Fig. 3).

3. Modelling approach and model description

Thorium isotopes have been used to investigate two processes in the oceans: that discussed here (i.e. constraining sediment and chemical fluxes to seafloor sediment) and also that of particle cycling within the water column. Several previous studies have developed elegant models of Th-isotope distribution in the water column in order to improve our understanding of the latter process (e.g. Clegg et al., 1991; Clegg and Whitfield, 1993; Murnane, 1994; Murnane et al., 1990). These models are markedly different from that developed here, and it is worth discussing how they function as an introduction to the model utilised in this study.

In order to understand the relatively rapid processes of particle cycling within the water column, models cannot make the assumption that chemical equilibrium occurs to give particulate and dissolved Th concentrations at the ideal Kd value. Instead, they must deal with adsorption and release as two independent processes. Also, as these models strive to understand particle dynamics, they require relatively complex particle handling. Ocean particles cover a wide range of sizes and therefore a wide range of settling rates. These various particle sizes are also interchangeable with one another because they stick together and fall apart. This complex behaviour is widely parametrized as a two-fold classification into fine, non-settling particles and coarse, rapidly settling particles, with exchange between these two occurring by aggregation and disaggregation. In a column of seawater, therefore, there are five kinetic processes occurring — adsorption, release, aggregation, disaggregation and particle settling. In order to understand this complex system, models require observations of dissolved

and particulate concentrations of several Th isotopes, particularly those that are short lived (^{228}Th, ^{234}Th), as well as particle concentration measurements. The complexity of these models, and the intense observational requirements, has so far limited them to one-dimensional cases.

By contrast, in order to assess the use of Th isotopes as a constant-flux indicator, much of this complexity can be simplified. Over the longer time-scales involved in Th

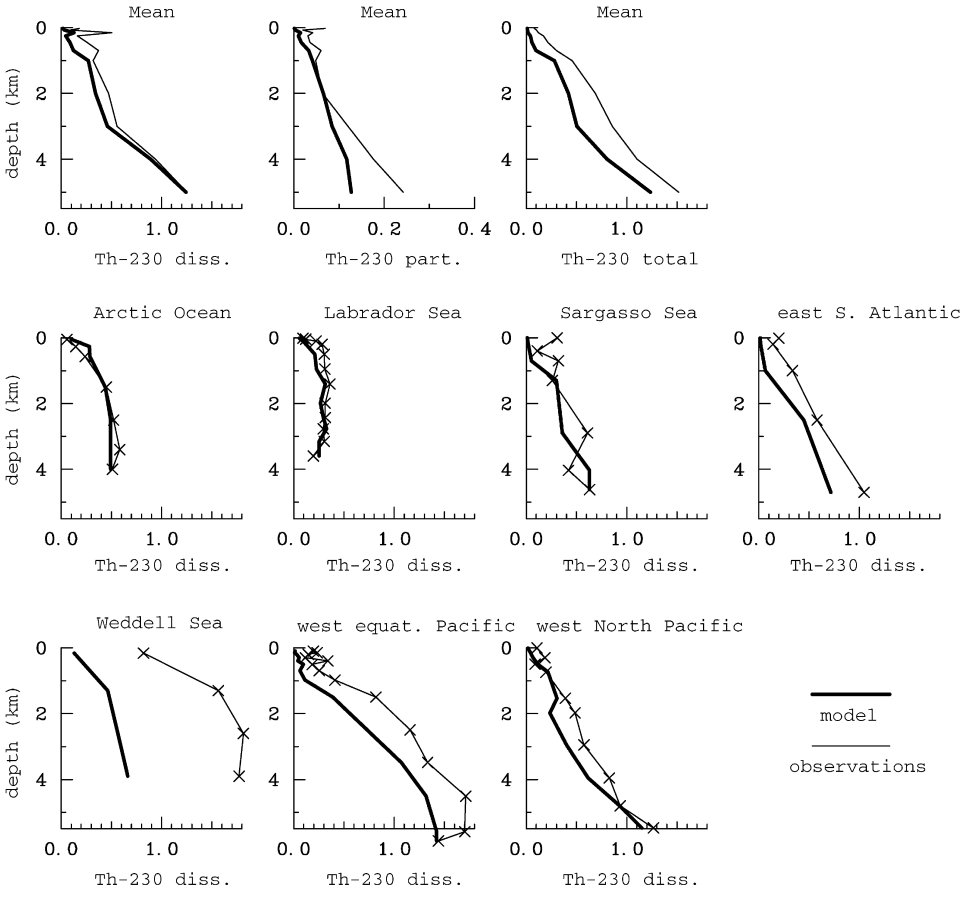

(a)

Fig. 3. Comparison of model and observed ^{230}Th profiles. The first three profiles of each panel compare the average depth profile of all observations with the average of model output at the same locations. The other seven profiles are representative of the observed profiles around the world (Fig. 2). The five panels show different runs of the model: (a) Holocene; (b) Glacial; (c) Sinking-Velocity sensitivity run (sinking velocity doubled from 3 to 6 m/d); (d) Kd value sensitivity run (Kd increased from solid line to dashed line in Fig. 1) and; (e) sea-ice sensitivity runs (upper panels — southern-hemisphere sea ice increased by 3.5° latitude, middle panels by 7.0°, and lower panels by 10.5°).

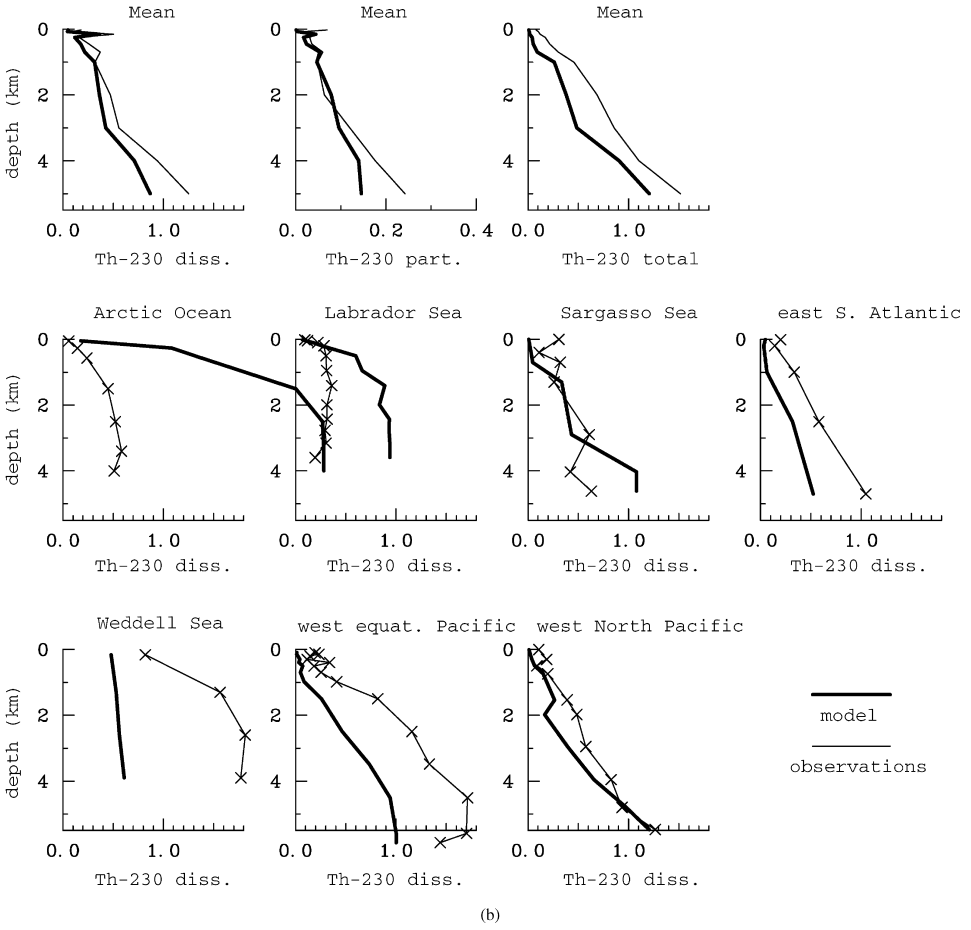

Fig. 3. (*continued*).

removal from the water column (years to tens of years), dissolved and particulate Th can be assumed to be in equilibrium at the Kd value. And particle cycling within the water column is also much less important such that, to a good approximation, the only important features for Th removal are the average settling velocity of particles through the water column and the Kd value. These simplifications allow the possibility of inserting a basic particle field and particle-reactive elements into existing three-dimensional GCMs.

In this study, we have done this using two well-documented GCMs developed by the Hamburg group. The first of these is the Hamburg Large Scale Geostrophic Ocean General Circulation Model (LSG-OGCM; Maier-Reimer et al., 1993), which derives ocean-circulation fields from basic fluid-dynamical principles. Derivation and performance of this model have been fully discussed (Maier-Reimer et al., 1993;

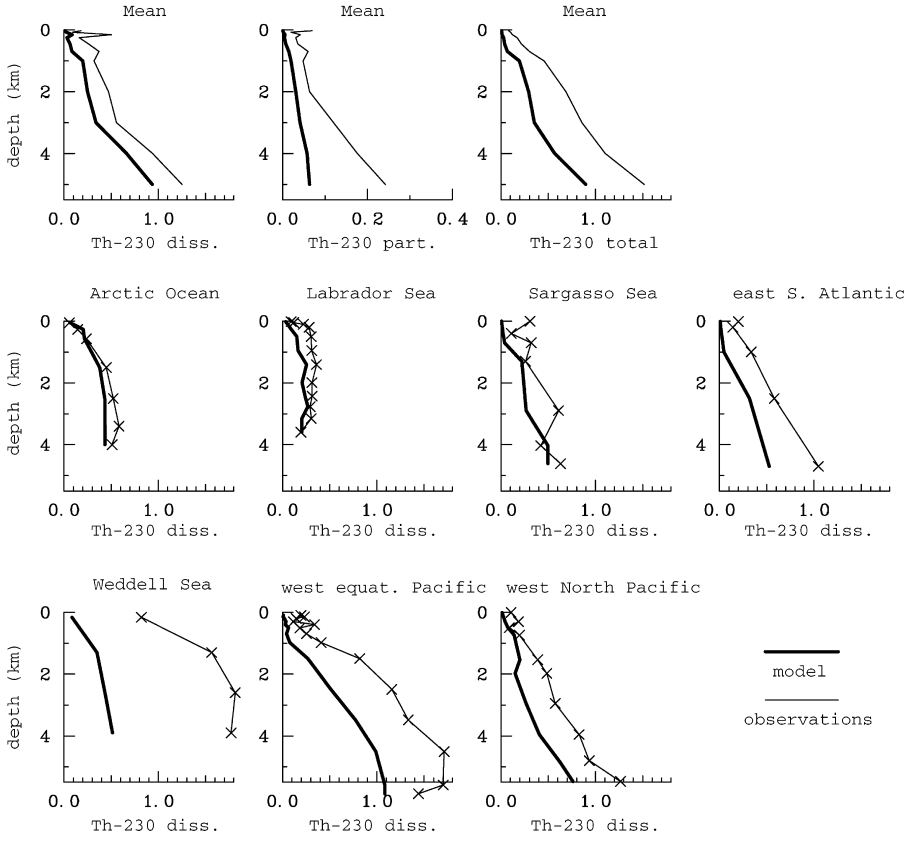

(c)

Fig. 3. (*continued*).

Winguth et al., 1996), and it provides velocity fields that correspond reasonably with those in the real world. For instance, the LSG-OGCM produces realistic salinity, density, and ^{14}C distributions in the oceans and creates 16 Sv of NADW. In this study, we use the pre-industrial fields of Winguth et al. (1996) for our Holocene simulation, because these fields can be directly compared with the circulation fields in response to glacial boundary conditions from the same study.

The LSG-OGCM velocity fields are then taken off-line and used in a carbon cycle model – the Hamburg Oceanic Carbon Cycle Model (HAMOCC), which is fully documented in Heinze et al. (1991) and Maier-Reimer (1993). This model uses the LSG-OGCM velocity fields to transport important chemical species (principally DIC, alkalinity, phosphate, oxygen, and silica) and predicts new production at the ocean surface of calcium carbonate, opal, and particulate organic carbon (POC) using Michaelis-Menten type production kinetics. In this study we use HAMOCC version

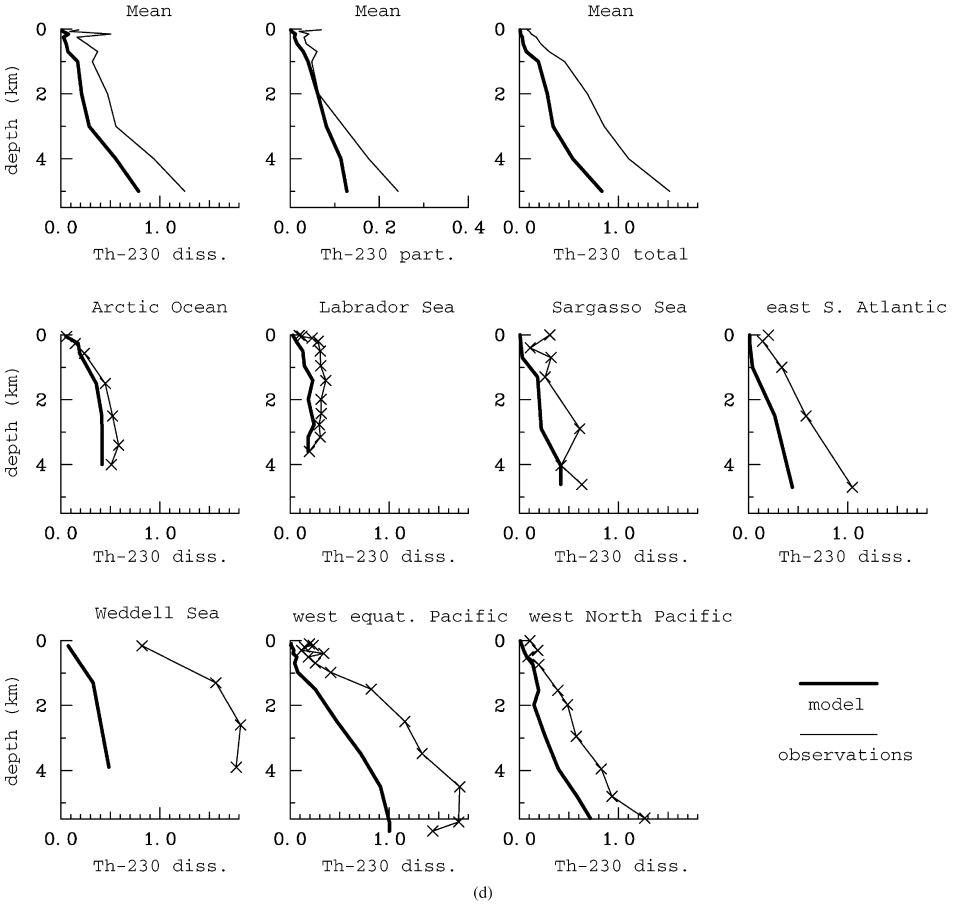

Fig. 3. (*continued*).

2 with an attached sediment model described in Heinze et al. (1999). We use a grid resolution of 3.5° latitude by 3.5° longitude, a time-step of one year, and 11 layers (which diminish in thickness upward in order to adequately describe the more complex surface processes). This resolution gives the model a total of $\approx$ 31,615 wet grid points (3452 wet grid points in the uppermost layer). This version of HAMOCC features, in addition to the three biogenic particle types, a terrigenous species of particle that is not involved in the carbon cycle. This consists of a uniform flux of dust to the surface ocean of 0.001 g/cm^2 kyr and is required to generate the terrigenous portion of deep-sea sediments in the sediment model of Heinze et al. (1999). This dust flux leads to rather low estimates for the terrigenous percentage of seawater particulate material averaging 1%. Observed values are higher than this, although they rarely exceed 10% except in regions of particularly high dust flux, such as beneath the Saharan dust plume. If the assumption that Th is scavenged equally to all

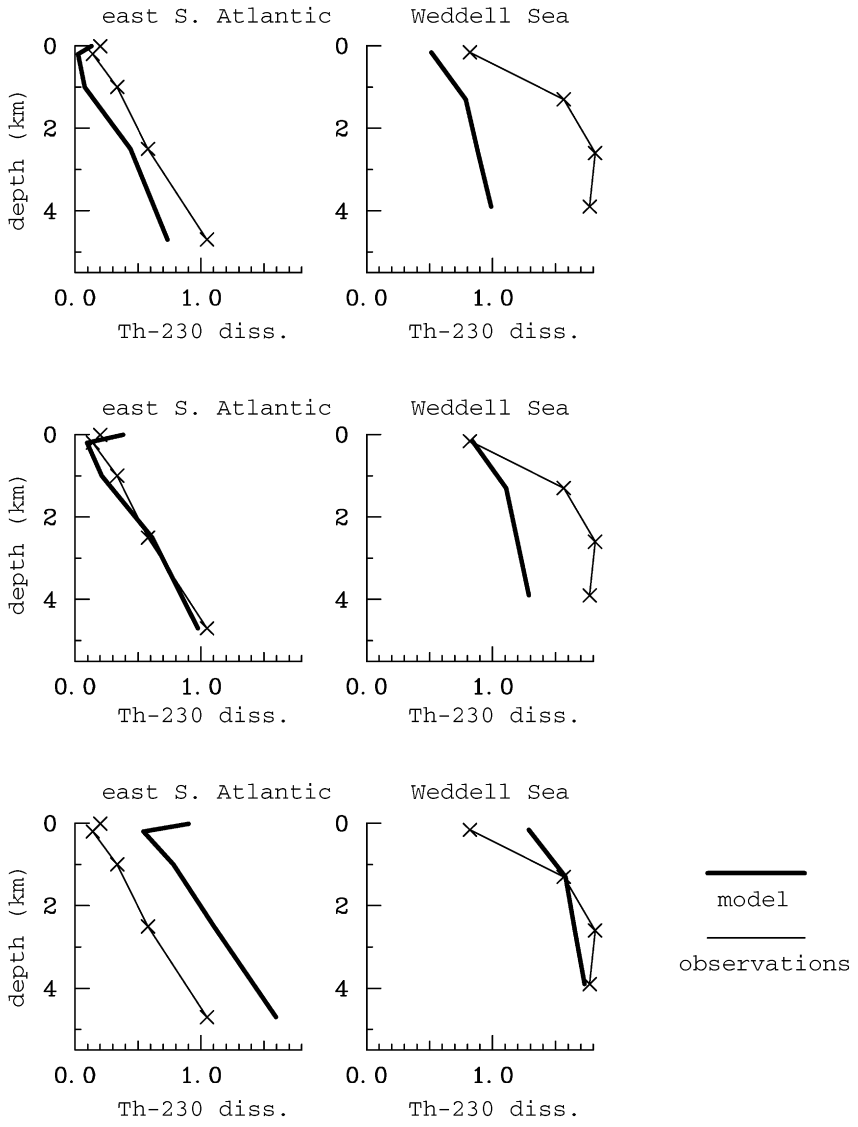

(e)

Fig. 3. (*continued*).

particles is correct and there is no preferential removal onto detrital material, then the fact that observed detrital fractions of particulate material are low means that underrepresenting this detrital fraction is not expected to cause a significant change in the pattern of Th scavenging.

Of key importance for the purposes of this study, model-derived new production of the three organic particle species (Maier-Reimer, 1993) and model-derived fluxes of material to the seafloor (Heinze et al., 1999) match those observed reasonably well.

In previously described versions of HAMOCC, particles were removed from the ocean surface directly to the seafloor with the only adjustment being for dissolution during descent. This strategy reflected the principal focus of this model as a CO_2 model: annual fluxes of carbon to the seafloor are important but the mechanism by which the carbon travels to the seafloor is not. In order to model particle-reactive species, however, we must create a realistic particle field and downward particle transport. The features of the model that does this are listed in Table 1 and are discussed in detail below.

We parametrize particle settling and the scavenging of ^{230}Th with a time-step shorter than 1 yr. The scavenging time-step is set by dividing the surface-layer thickness by a prescribed average particle-settling rate. In other words, the time it takes an average particle formed at the surface to leave the surface layer of the model prescribes the length of the scavenging subroutine time-step, t:

$$t = L_1/S \tag{1}$$

where L_1 is the thickness of the surface layer in the model (50 m), and S is the average settling rate (for which a value of 3 m/d was used in this study as discussed below). The mass of particles produced during this time-step is calculated for each surface-layer grid point from the HAMMOC annual new production. This mass of particles is distributed throughout the surface layer to give a particle concentration:

$$M_{\text{part.}} = Pt/L_1 \tag{2}$$

where M_{part} is the particle concentration (g/l) and P is the new production. We assume a uniform settling rate for all grid points and all depths. The validity of this assumption and the effect of deviation from it are assessed in a later section.

Thorium-230 is produced in the model every timestep, t, at the rate known from decay of U (0.0468 atoms/sl; Chen et al., 1986). Once produced, it advects and diffuses

Table 1
Summary of operation of scavenging GCM

A. Flow fields and particle production read in from LSG-OGCM and HAMMOC
   Variables (Kd and particle settling rate) entered
B. Timestep t (runs many times per year) — 1 dimensional for each lat. and long.
   (i) particle concentration calculated for layer one
   (ii) ^{230}Th produced from U decay
   (iii) particles and $^{230}Th_{part}$ settle to next layer with correction for dissolution
   (iv) ^{230}Th re-equilibrated
C. Annual timestep — 3 dimensional
   (i) radioactive decay of ^{230}Th
   (ii) advection and diffusion of water and $^{230}Th_{diss}$
D. Return to B, unless model has achieved steady state

with the water mass it is formed in, within the main model and therefore with an annual time-step. Thorium-230 decay is accounted for within the annual time-step but is insignificant due to the short residence time of ^{230}Th. Thorium-230 scavenging is performed within the scavenging subroutine assuming equilibrium is achieved and using the Kd values shown in Fig. 1. A slight downward correction of the best fit relationship of Honeyman et al. (1988) from $\mathrm{Kd} = 7.2 - 0.42.\log_{10}$(particle-mass) to $\mathrm{Kd} = 7.0 - 0.42.\log_{10}$(particle-mass) was applied to achieve an improved reproduction of the observed values, but this is still compatible with the observations. The model's sensitivity to small changes in the Kd value is discussed in a later section. The Kd is defined by:

$$\mathrm{Kd} = \frac{^{230}\mathrm{Th}_{\mathrm{part.}}/M_{\mathrm{part.}}}{^{230}\mathrm{Th}_{\mathrm{diss.}}/M_{\mathrm{water}}} \tag{3}$$

where $^{230}\mathrm{Th}_{\mathrm{part.}}$ = activity of ^{230}Th attached to particles (dpm/l), $^{230}\mathrm{Th}_{\mathrm{diss.}}$ = activity of ^{230}Th in solution (dpm/l); M_{water} is the mass of seawater per litre; and $M_{\mathrm{part.}}$ is the mass of particles per litre. The Kd value is prescribed, M_{water} known, and $M_{\mathrm{part.}}$ calculated from HAMOCC productivity fields with Eq. (2). The numerical scheme for equilibration between dissolved and particle-attached ^{230}Th is then given by the four equations below. Superscripts "old" "inter" and "new" indicate the activities at the previous time-step; prior to equilibration; and after equilibration respectively. $^{230}\mathrm{Th}_{\mathrm{settle}}$ is the total ^{230}Th added from the grid point above by settling particles; U decay is the ^{230}Th addition from U decay; and $^{230}\mathrm{Th}_{\mathrm{adv.}}$ is the net input to the grid point due to advection of $^{230}\mathrm{Th}_{\mathrm{diss}}$ from adjacent grid points. Note that the final term of Eq. (4) is included only once every model year while all other features of the equilibration occur with a faster timestep, t.

$$^{230}\mathrm{Th}^{\mathrm{inter}}_{\mathrm{diss.}} = {}^{230}\mathrm{Th}^{\mathrm{old}}_{\mathrm{diss.}} + {}^{230}\mathrm{Th}_{\mathrm{settle}} + \mathrm{U\ decay} + {}^{230}\mathrm{Th}_{\mathrm{adv.}} \tag{4}$$

$$^{230}\mathrm{Th}^{\mathrm{new}}_{\mathrm{diss.}} = {}^{230}\mathrm{Th}^{\mathrm{inter}}_{\mathrm{diss.}} - \Delta x \tag{5}$$

$$^{230}\mathrm{Th}^{\mathrm{new}}_{\mathrm{part.}} = {}^{230}\mathrm{Th}^{\mathrm{old}}_{\mathrm{part.}} + \Delta x \tag{6}$$

where:

$$\Delta x = \left[\frac{\mathrm{Kd} \times M_{\mathrm{part.}} \times {}^{230}\mathrm{Th}^{\mathrm{inter}}_{\mathrm{diss.}}/M_{\mathrm{water}} - {}^{230}\mathrm{Th}^{\mathrm{old}}_{\mathrm{part.}}}{(\mathrm{Kd} \times M_{\mathrm{part.}}/M_{\mathrm{water}}) + 1} \right]. \tag{7}$$

This yields concentrations in the particulate material ($^{230}\mathrm{Th}_{\mathrm{part}}$) and in the water ($^{230}\mathrm{Th}_{\mathrm{diss}}$). For the surface layer, all particles and therefore all $^{230}\mathrm{Th}_{\mathrm{part}}$, settle to the layer below. In this second layer, and all subsequent layers, particle concentrations and downward fluxes (F) are adjusted for particle dissolution. We use exponential penetration profiles to parametrise dissolution and remineralisation (Volk and Hoffert, 1985; Najjar et al., 1992; Maier-Reimer, 1993):

$$F(z) = F(z_0) \cdot \mathrm{e}\left(\frac{z_0 - z}{z_p}\right) \tag{8}$$

where z is the water depth, z_0 the lower boundary of the euphotic zone (in the model, the lower boundary of the uppermost layer, i.e. 50 m) and z_p the penetration depth at which the export flux is reduced to 1/e that out of the euphotic zone. In the model, z_p is set to 770 m for POC; 2000 m for calcium carbonate; and 10,000 m for opal. Particles that re-dissolve release their ^{230}Th to seawater (i.e. adding to $^{230}Th_{diss}$). Remaining $^{230}Th_{part}$ is included in the calculation of equilibrium $^{230}Th_{part}$ and $^{230}Th_{diss}$ for that layer. For layers other than the surface layer, the flux of particulate ^{230}Th downward to the next layer is calculated from the concentration of ^{230}Th on particles (dpm/g) and the downward particle flux.

Although $^{230}Th_{diss}$ is treated in a true three dimensional sense and can advect and diffuse, particle settling and $^{230}Th_{part}$ is dealt with largely as a one dimensional system for each grid point. This is justified because particles settle through the entire water column fast enough that they do not have time to be advected far beyond the grid point in which they form before they reach the seafloor. The exception to this one-dimensional case is POC, which is allowed to advect in the model. Test runs with increased floating POC produced no significant difference in the pattern of ^{230}Th scavenging except in the eastern equatorial Pacific, where unrealistic nutrient trapping caused too high a POC concentration and therefore too high a $^{230}Th_{part}$ value. This nutrient trapping has been discussed previously by Najjar et al. (1992) and Maier-Reimer et al. (1992).

Several model runs will be discussed in this study. The first, termed "Control", uses a carbon cycle exactly equivalent to that in Heinze et al. (1999) but simply features the addition of the scavenging subroutine. On the basis of this model's ability to mimic water-column ^{230}Th observations, two adjustments were made before the second "Holocene" run. The first adjustment was that particle productivity was introduced under sea-ice as, without it, the dissolved ^{230}Th values were clearly too high. The LSG-OGCM contains a simple thermodynamic ice model (Maier-Reimer et al., 1993), which produces ice-cover close to that observed for the Holocene and close to the CLIMAP reconstruction for the Glacial (CLIMAP, 1981). Possible problems with this ice model are discussed in the "Water column ^{230}Th distributions" section below. Productivity under ice was parametrised as identical to no-ice productivity when the ice was < 1 cm thick. When ice was > 1 cm thick, nutrient-uptake rates in the productivity equation (Heinze et al., 1999) were divided by ice thickness in cm. The second change was an increase of the POC remineralization rate from 20 to 2 yr in order to solve the nutrient-trapping problem discussed in the previous paragraph.

The third run is a sensitivity study of the effect of speeding up the rate of particle settling and is termed "Sinking velocity". In the fourth run (labelled "Kd value") we test how sensitive the model distributions are to small changes in the Kd value. Several further runs test the model's sensitivity to the ice-model. And the final run makes use of the velocity and productivity fields of the last glacial maximum (LGM) versions of the Hamburg model (Winguth et al., 1996) to yield a "Glacial" run. The LGM version of the model has boundary conditions derived from an atmospheric GCM and δ^{18}O measurements of LGM foraminifera. Considerable uncertainty exists about LGM ocean circulation, but the model reproduces the main features of the past

$\delta^{13}C$ features and reduces the Atlantic conveyor belt by about half, in line with expectations (Winguth et al., 1996).

For ^{230}Th, the model comes into equilibrium with an e-folding time roughly equivalent to the residence time of ^{230}Th, so runs as short as only a few hundred years are in equilibrium. In practice, therefore, run lengths are controlled by equilibration of the carbon system. Fifty thousand years of integration time were used for the carbon-cycle system, while the Th experiments were integrated for 2000 yr. Restarting from zero concentrations for Th, the major adjustment towards equilibration is accomplished after 200 yr, so these run lengths are ample to achieve full equilibrium.

4. "Holocene" model results

4.1. Particle distributions and fluxes

There have been a large number of studies of particle concentration in the oceans, but rather few of these present data for large regions. The best studied ocean basin in this respect is the Atlantic, for which there are two basin-wide studies (Biscaye and Eittreim, 1977; Brewer et al., 1976; Fig. 4). One of these studies is based on nephelometer readings (Biscaye and Eittreim, 1977), which have the advantage of sampling a large volume of water and for which there are over 1000 reported stations measured over a number of years and through all seasons. This study is therefore considered to give the more robust estimate of the relative distribution of particle concentrations. However, nephelometer readings are based on light scattering, and the conversion to actual particle concentration is subject to considerable uncertainty. While relative particle concentrations in the nephelometry study are likely to be robust, the absolute values are less so.

The Brewer et al. (1976) study is based on direct measurements of the particulate content of seawater performed by filtration and weighing. It has the disadvantages, however, that it is based on only some 30 profiles collected sequentially north to south in a single year (July 1972–January 1973) and consists of measurements of only 10–20 l of water. This introduces the possibility that there is seasonal biasing in the data, or that individual measurements are not representative of the long-term value at any particular site. In particular, it is curious that this study does not report a significant maximum in particle concentration around the equator, as the Biscaye and Eittreim (1977) study shows a strong maximum here, which is also to be expected from the high productivity in this region. This omission partially reflects the lack of a sampling station directly at the equator in the Brewer et al. (1976) study.

Combining these studies, stressing the absolute values of the direct measurements and the pattern of the nephelometry study, the most important features of the particle distribution in the Atlantic are as follows:

1. At depths greater than 1000 m in the gyres, concentrations are low at around 12 μg/l.
2. At high latitude and at the equator, deep-water concentrations are up to four times higher than this.

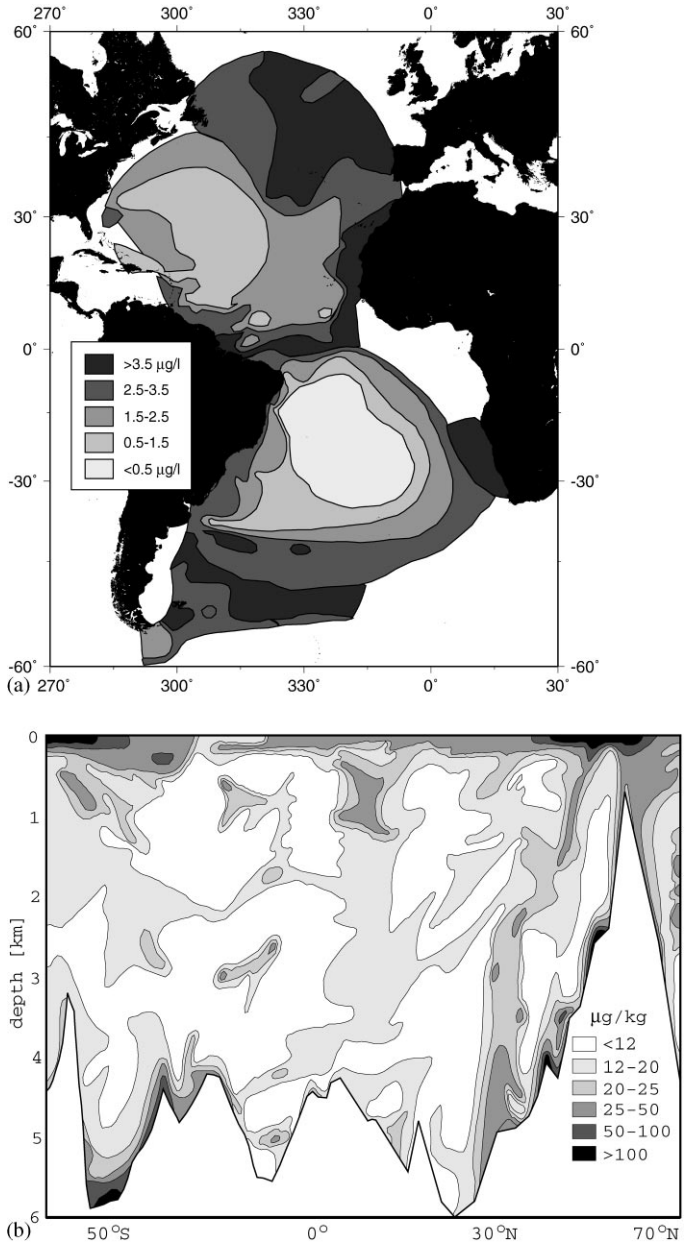

Fig. 4. Particle concentrations for the Atlantic. (a) particle concentrations at middepth in the water column ($\approx$ 2–3 km) based on nephelometry (Biscaye and Eittreim, 1977); (b) Directly measured values along the W. Atlantic GEOSECS section (Brewer et al., 1976); (c) model output for the Holocene run of this study for the same W. Atlantic GEOSECS section (see small panel for location of this section).

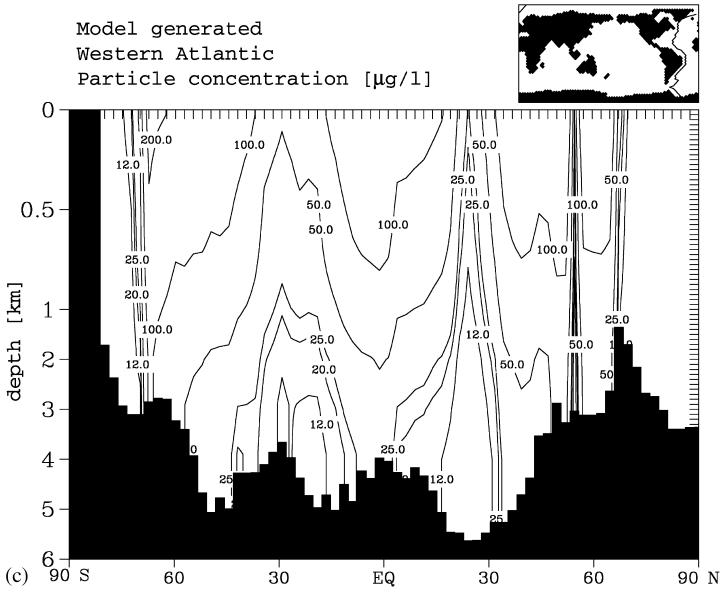

Fig. 4. (*continued*).

3. In the surface ocean, concentrations are still higher, generally greater than 50 µg/l and sometimes as high as 200 µg/l.
4. There is a tendency for the North Atlantic to have higher particle concentrations than the south.
5. Just above the sediment-water interface in the western margin of the basin, nepheloid layers significantly increase the particle concentrations.

Model-derived particle concentrations duplicate the first three of these observations (Fig. 4c). The pattern of particle concentration in the model is controlled by surface productivity, while the absolute values are controlled by dissolution and by the chosen settling rate.

The lack of higher particle concentrations in the North Atlantic within the model reflects the simplistic input of terrigenous material in the model. This model-observation discrepancy is not expected to make a large difference to the pattern of ^{230}Th scavenging. Nepheloid layers are not explicitly included in the model. Particles resuspended into the bottom of the ocean have already come into equilibrium with bottom water, so they are not expected to significantly increase the removal of ^{230}Th from the dissolved phase, although they will obviously increase $^{230}Th_{part}$.

4.2. Water column ^{230}Th distribution

"Holocene" run values of $^{230}Th_{diss}$ and $^{230}Th_{part}$ match observations reasonably well (Fig. 3a). Average model profiles of dissolved, particulate and total ^{230}Th show

a steady increase in ^{230}Th with depth as dictated by the reversible scavenging process. The rate of increase for all three profiles fits well with those of the observations. $^{230}Th_{part}$ values are somewhat underestimated in deep water due to the lack of a nepheloid layer in the model, but this represents a higher standing stock of $^{230}Th_{part}$ and probably does not alter the vertical Th fluxes.

The closeness of the fit to the observed data is firm support that the model is doing a good job of mimicking the real behaviour of ^{230}Th. All three model profiles show a kink at 3 km. This is not real and reflects lack of resolution in the deeper sections of the model (for comparison of the mean profiles, the observed data were interpolated onto the model layer standard depths).

More interesting than the average profiles are the comparisons between the model and individual profiles (Fig. 3).

Arctic ocean: The profile chosen for comparison here is from the Nansen Basin (Cochran et al., 1995). In this basin, particle fluxes are low, which might be expected to lead to rapidly increasing ^{230}Th concentrations with water depth. While this is seen high in the water column, the profile steepens at depth. Cochran et al. (1995) suggested that this was due either to the known rapid ventilation of this basin causing low-^{230}Th surface waters to be carried to depth, or to increased scavenging of ^{230}Th at the slopes surrounding the basin. The model $^{230}Th_{diss}$ profile fits the observations well (Fig. 3a). Although the absolute value of the model profile is somewhat tuneable by changing under-ice productivity, the shape of the profile is not. As the close fit is achieved without enhanced slope scavenging in the model, this suggests that ^{230}Th in this region can be explained by ventilation of low ^{230}Th waters to depth. Enhanced slope scavenging may occur but is not necessary to explain the data. Elsewhere in the Nansen Basin the fit to the data is also good. In the Amundsen and Makarov basins, however, the model tends to predict $^{230}Th_{diss}$ higher than that observed (Scholten et al., 1995). This probably reflects the oversimplified under-ice productivity and detrital dust fluxes of the model resulting in too few particles in this region.

Labrador Sea: This profile is taken from Moran et al. (1997) and shows a roughly constant value with depth at only ≈ 0.3 dpm/1000 l. This profile was interpreted by the authors as due to the rapid advection of surface water to depth by NADW flow. The model profile duplicates that measured for precisely this reason. This provides one of the more convincing indications that the model is advecting ^{230}Th in a realistic manner and clearly supports the idea that advection of ^{230}Th is an important process, at least in the North Atlantic.

Sargasso Sea: This profile, from Cochran et al. (1987), is somewhat noisy but shows values higher than in the Labrador Sea and with a tendency to increase with depth. Values are not as high, however, as those seen further south in the Atlantic or in the Pacific Ocean. This profile can be interpreted as reflecting the gradual build-up of ^{230}Th in NADW as it travels southward. The model fit is good given the noisiness of the data.

Eastern South Atlantic: This far south in the Atlantic, a more linear ^{230}Th profile has been established (Rutgers van der Loeff and Berger, 1993), which increases to values higher than those further north. The model also shows a linear increase, but values are slightly lower than those observed. As much of this difference occurs in the upper water column, this may reflect the slightly higher particle concentrations in the model

compared to those observed in this region. Alternatively, it may be caused by the problem discussed in the next paragraph.

Weddell Sea: This region is that most poorly captured by the model. The profile shown (from Rutgers van der Loeff and Berger, 1993) is the worst example of the model deviating from observations. Observed values are much higher than elsewhere in the Atlantic and are some of the highest measured anywhere in the oceans. Rutgers van der Loeff and Berger (1993) attribute this to upwelling of high-^{230}Th ACC deep water into the Weddell Sea coupled with low particle fluxes. The discrepancy between the model and observations must mean that the model's circulation field or particle handling are not adequate descriptions of those observed in the region. One potential culprit is that under-ice productivity in the model is too high. Turning off all productivity under the ice, however, makes almost no difference to the model's Weddell Sea ^{230}Th profile (as shown in the "control run"). As a further investigation of this possibility, we tried three additional runs, in which the sea-ice boundary was moved progressively northward by one model grid point and productivity was kept at zero under any ice-covered region. Model profiles for the east south Atlantic and the Weddell Sea are shown from these three runs in Fig. 3e. As the sea-ice cover is extended further north, dissolved ^{230}Th increases so that the eastern south Atlantic profile is matched with 7° of extra ice cover and the Weddell Sea profile is matched with 10.5° extra ice cover. It is possible that the ice model is underrepresenting southern hemisphere ice cover, and this may go some way towards explaining the model-observation discrepancy here. However, it is very unlikely that the model's sea-ice is incorrect by the magnitude required to bring the model into agreement with the Weddell Sea observations. This implies that there is an additional problem with the model. The most plausible explanation is that the model's lateral mixing between the ACC and the Weddell Sea is too strong and that this smooths out the high ^{230}Th values that should occur in the far south. High lateral mixing arises due to the lack of a well described frontal system in the model Southern Ocean. This is a general problem with ocean GCMs and is caused by insufficient model resolution to accurately capture the processes of deep-water formation. This problem means that model results from the far Southern Ocean are not trustworthy. However, as this problem is unique to the far Southern Ocean, it does not affect the validity of the results in the rest of the ocean.

Western Equatorial Pacific: This profile, measured by Nozaki and Nakanishi (1985), shows the typical increase of ^{230}Th with depth but to values rather higher than seen in the Atlantic. This presumably reflects the relatively greater age of the water here coupled with the low productivity in the region. The general increase and high values are reproduced by the model.

Western North Pacific: This profile (Nozaki et al., 1981) exhibits lower ^{230}Th values than the previous one, reflecting the higher productivity of the region. This basic feature is captured by the model, although the increase is not as monotonic as that observed, probably due to small amounts of unrealistic mid-depth ventilation in the model.

With the exception of some ice-covered regions, particularly the Weddell Sea and some Arctic basins, the model replicates the observations reasonably well. Given the

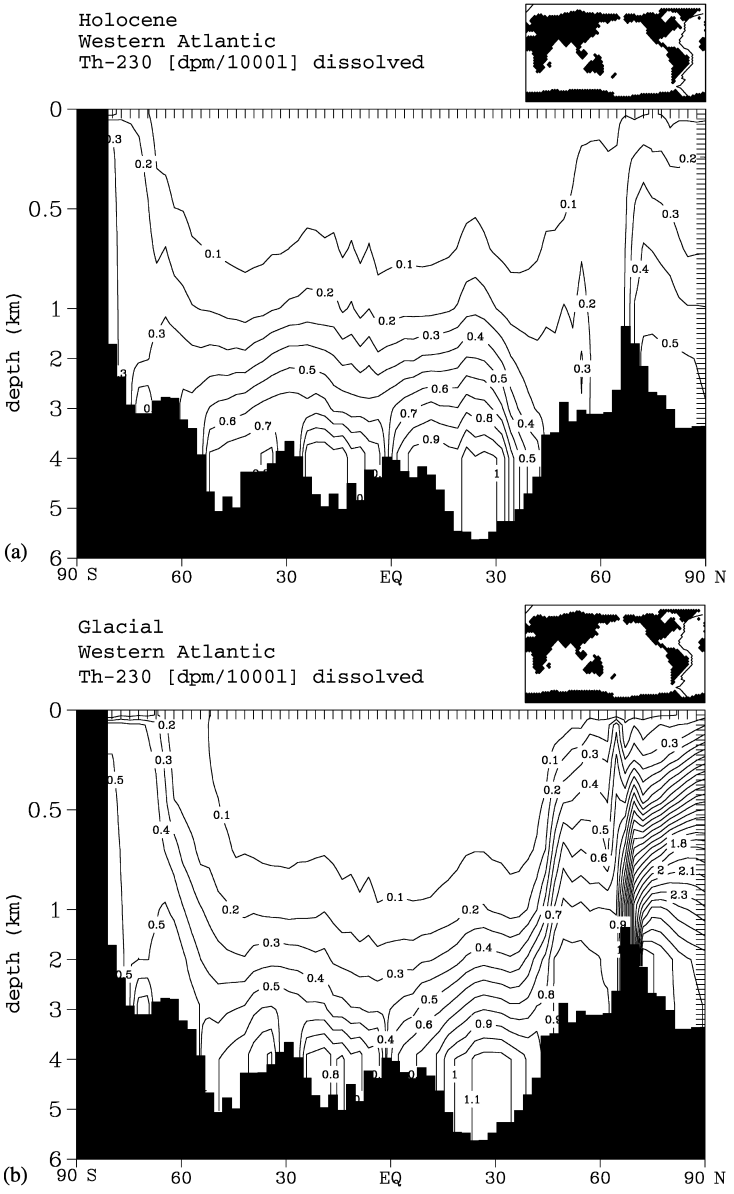

Fig. 5. Model-derived $^{230}Th_{diss}$ sections for the Western Atlantic. (a) Holocene and (b) Last Glacial Maximum.

coarseness of the model resolution, the degree of fit is pleasing and suggests that predicted model ^{230}Th values for other regions of the ocean are also valid. An example of model-predicted $^{230}Th_{diss}$ concentrations is shown in Fig. 5a for the Western Atlantic. For much of this section, the value increases roughly linearly with depth. In

the North Atlantic the effect of NADW is shown by the advection of low ^{230}Th waters to depth.

4.3. ^{230}Th flux to sediment

The quality of the fit between the model and the water-column observations, both of particle concentrations and of ^{230}Th, is sufficiently good to suggest that the model is well replicating the advection and scavenging of ^{230}Th. This enables us to construct a global map of the expected ^{230}Th flux to the sediment from the model (Fig. 6a). Values in this map have been normalised to the production in the overlying water column such that values >1 signify that more ^{230}Th enters the sediment than is produced in the overlying water.

Ignoring the far Southern Ocean (where the model is inadequate at replicating water-column ^{230}Th distributions) the normalised ^{230}Th flux ranges from 0.4 to 1.4. In general, high values are seen in the more productive regions as is to be expected due to the higher particle fluxes. Most of the Arctic Ocean exhibits low ^{230}Th flux. This has been observed as low ^{230}Th inventories in Arctic sediments (e.g. Ku and Broecker, 1967) and is due to the low particle flux here possibly coupled with the ventilation of low ^{230}Th surface waters to depth. This low ^{230}Th flux is balanced by intense scavenging in small areas of the basin, particularly just north of the Bering Straight, where the annually averaged sea-ice thickness is small and hence biological production is sizeable leading to higher particle concentrations than in the central Arctic. The mixing of water in the Arctic Ocean carries ^{230}Th to this area of relatively high particle flux to be scavenged.

The short residence time of deep waters in the Atlantic and their rapid advection southward means that the western North Atlantic features a ^{230}Th flux lower than that expected from production. The ^{230}Th not scavenged here is carried southward to be removed in the productive equatorial belt and in the southern Atlantic. For the Southern Ocean, some care must be taken in interpreting the flux map as values in the far south are not trustworthy. But values to the north of the peak of scavenging are expected to be robust and the general pattern of normalised ^{230}Th fluxes greater than 1.0 in this region, particularly in the Atlantic and Indian sectors, is expected to be correct. This region is acting as the major sink for ^{230}Th advected southward from the Atlantic. In the Pacific ocean, where this advection is not present, the Southern Ocean productivity belt still features high ^{230}Th fluxes but with values considerably lower than in the Atlantic and Indian. Elsewhere in the Pacific, contrasts between productive and gyre regions are as strong as seen in the Atlantic. In particular, values as low as 0.4 are seen in the South Pacific gyre and as high as 1.4 in the productive northwest Pacific.

Away from the far Southern Ocean, we consider the values on this flux map to be reasonably robust. They are derived using two well documented GCMs known to get the major features of circulation and productivity correct; they use well-understood Th scavenging processes; and a settling rate set to a realistic value. Furthermore, the model generates reasonable oceanic particle fields and a good fit to the water column ^{230}Th data. Developmental work on the model clearly demonstrated that the

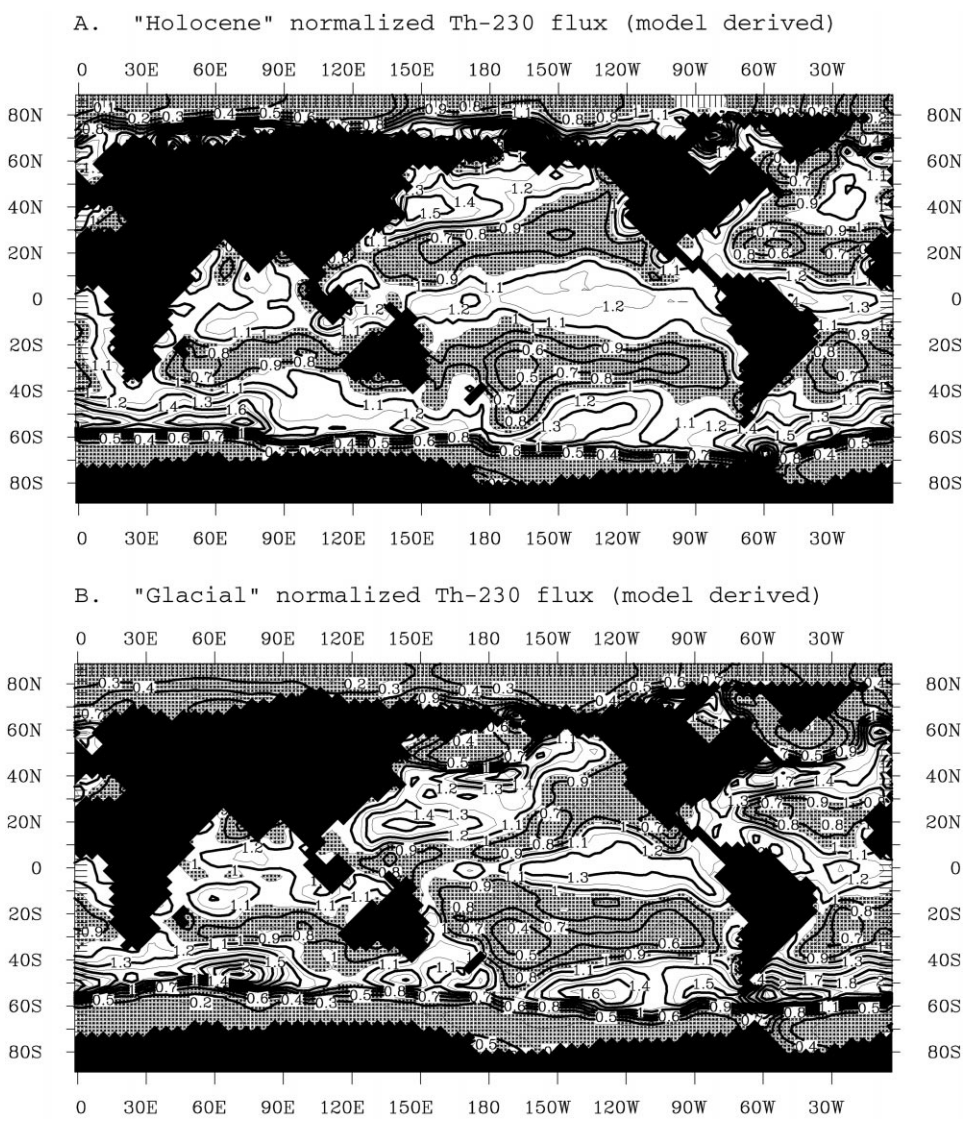

Fig. 6. Thorium-230 flux-to-sediment, normalised to the production in the overlying water column. Shaded areas represent those regions were the flux is less than the production and there is therefore net transport of ^{230}Th away from these regions to the non-shaded regions. (a) Holocene; (b) Glacial; (c) Sinking-Velocity sensitivity run (sinking velocity doubled from 3 to 6 m/d); (d) Kd-value sensitivity run (Kd increased from solid line to dashed line in Fig. 1); and (e) Glacial minus Holocene.

water-column ^{230}Th distribution is more sensitive to changes in model parameters than is the flux to the sediment of ^{230}Th, so the quality of the model fit to the observed water-column data is particularly reassuring.

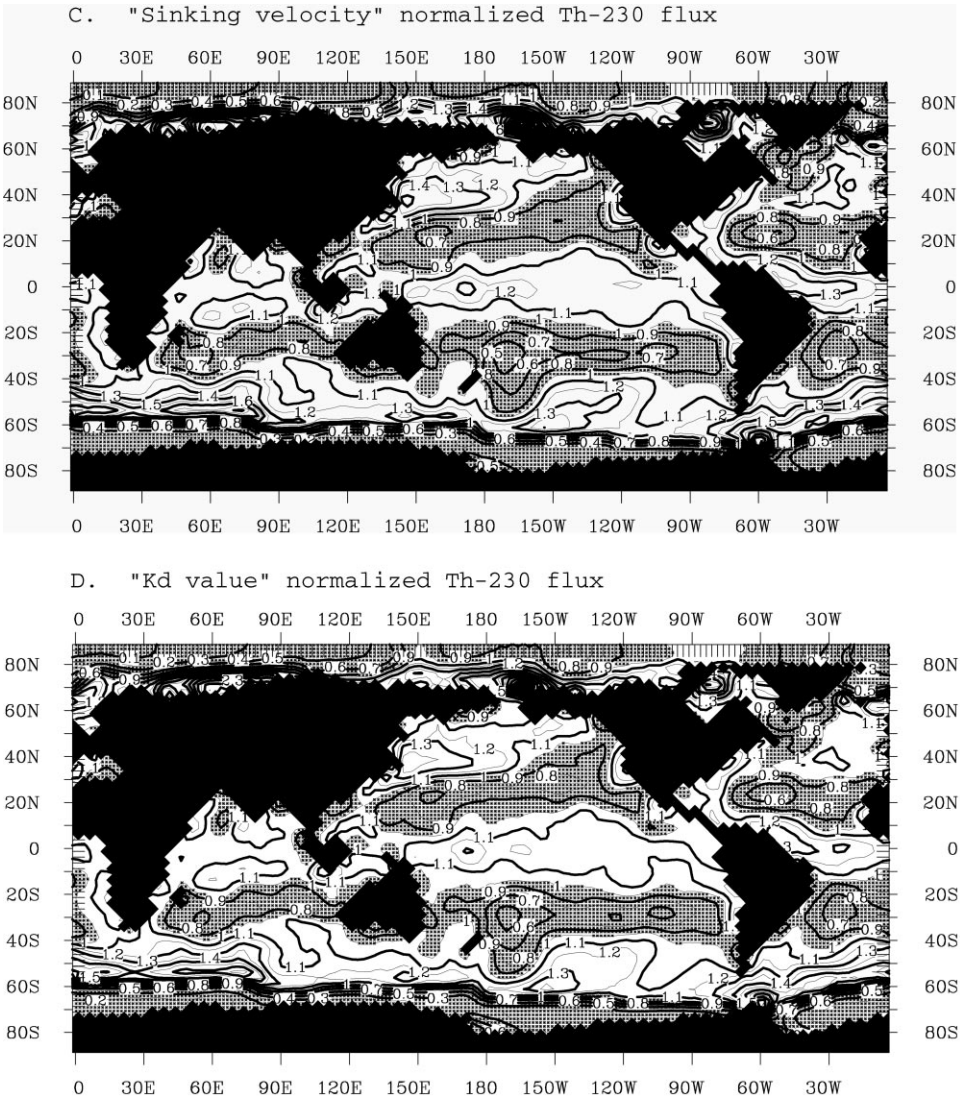

Fig. 6. (*continued*).

Comparing the model data to measured flux data is difficult. Of the sediment-trap studies of ^{230}Th fluxes, about half were specifically designed to test the near-shore effects of boundary scavenging (Anderson et al., 1983a,1994; Lao et al., 1993), something we have not attempted to replicate. Many of the remaining, open-ocean, studies have reported trouble with incomplete or over-efficient trapping of material. For instance Brewer et al. (1980) reported trap efficiencies ranging from 20 to $>98\%$ calculated using a range of nuclide fluxes, and Colley et al. (1995) reported significant

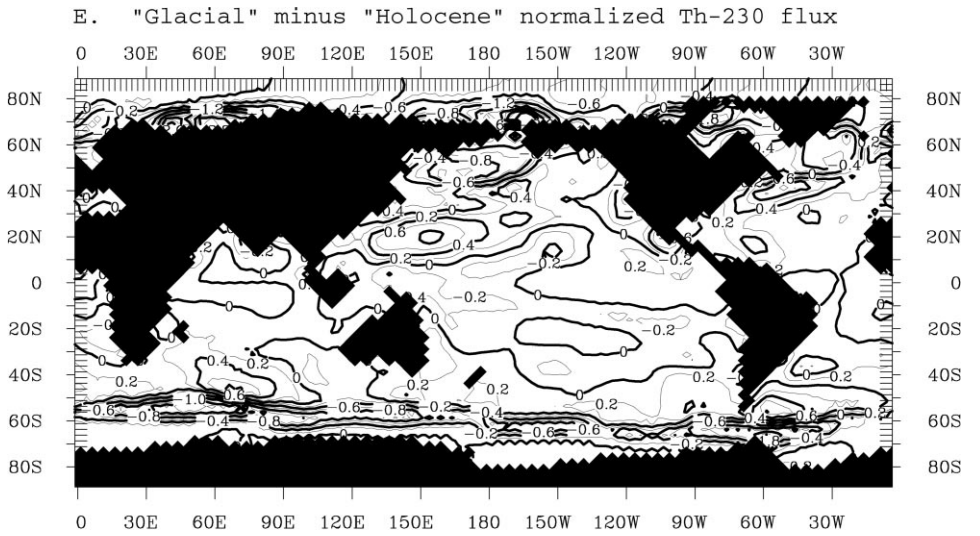

Fig. 6. (*continued*).

trapping of ^{230}Th from resuspended sediment in a trap close to the seafloor. In general, open-ocean ^{230}Th trap fluxes are less than the production ratio, averaging about 0.66 (Anderson et al., 1983b; Bacon et al., 1985; Colley et al., 1995; Taguchi et al., 1989). Detailed modelling of particle cycling and ^{234}Th scavenging has also suggested that sediment traps under-estimate ^{234}Th and sediment fluxes (Clegg and Whitfield, 1993). In general, there appears to be some agreement that traps have a tendency to under collect the finer particles from seawater and therefore, presumably, to under collect ^{230}Th. This has led to the use of trap ^{230}Th fluxes to assess their collection efficiency in order to correct other fluxes.

Another problem is that sediment traps are generally not deployed for a full year and therefore suffer from seasonal bias. A good example is the study of Taguchi et al. (1989), who reported fluxes of ^{230}Th for the highly productive North Pacific but with a deployment period that did not encompass the annual bloom. Comparing these results with the annual mean calculated by the model in this study is therefore not valid. Although sediment traps are of great use in determining ratios of nuclides in settling particles (e.g. ^{231}Pa/^{230}Th), they are clearly less reliable for measuring fluxes of ^{230}Th. Perhaps the most reliable sediment-trap study of ^{230}Th is that of Bacon et al., 1985, which involved deployment of a sediment trap close to Bermuda for the majority of a complete year. The authors considered the trap to be $105 \pm 17\%$ efficient, and it yielded a ^{230}Th flux/production ratio of 0.71. This compares to a model output for the area of 0.8, in reasonable agreement.

Measurement of the flux of ^{230}Th into sediment by direct analysis of that sediment are complicated by the process of sediment focusing and are therefore also difficult to use as true estimates of the ^{230}Th flux out of the water column. The estimates derived

from this modelling study therefore present probably the best attempt to constrain the variability of the flux of ^{230}Th to the sediment. Variability about the ideal no-advection case does occur to yield a ^{230}Th flux/production ratio ranging between 0.4 and 1.4. In many areas of the ocean the model predicts a deviation that is much smaller than this and suggests that 71% of the ocean exhibits a flux within 30% of that expected from production. 30% is the value commonly cited as the uncertainty on the use of ^{230}Th normalisation, so nearly three quarters of the ocean is expected to achieve previously quoted levels of uncertainty. In the remaining quarter of the oceans, however, where productivity is unusually high or low, the process of advection of ^{230}Th can yield ^{230}Th-normalised flux values that deviate more significantly from production.

4.4. Particle settling rates and model sensitivity

In this section we compare our best-fit value of the particle settling rate with observations and then discuss the effect on model output of varying this parameter both globally and by introducing regional variability.

Most modelling of ocean particles has divided them into fine, non-settling particles and large particles, which settle through the water column at rates of 100–150 m/d (Bacon et al., 1985; Clegg et al., 1991; Clegg and Whitfield, 1991; Cochran et al., 1993; Nozaki et al., 1987). Attempts to independently constrain this large-particle settling rate have yielded slower values of $\approx$ 20 m/d (Brewer et al., 1980; Murnane et al., 1990). Large particles, however, constitute only a small fraction of the total particle mass in the water column at any one time. Average settling rates for all particles are best estimated from water-column measurements of particle-reactive nuclides rather than measurements of sediment trap material, which capture only rapidly settling particles. Nuclide-based estimates of settling rates made from water-column profiles range from 0.2 to 5.3 m/d (Krishnaswami et al., 1976b; Mangini and Key, 1983; Tsunogai and Minagawa, 1978). The value used in this study to give a good fit to ^{230}Th observations and a realistic particle field is 3 m/d. This is in the middle of the existing range of estimates, which indicates the internal consistency of the model and argues for the validity of its results.

Increasing the rate at which particles settle in the model reduces water-column particle concentrations and ^{230}Th concentrations. As the productivity of the surface ocean is set at the observed level by the HAMOCC model, the flux of particle mass per year is also set. So an increase of the settling rate means that there is less particle mass suspended in the water column. Such an increase therefore causes the model to replicate the observed particle concentrations less well. Lower particle concentrations obviously also lower $^{230}Th_{part}$ in the water column. At lower particle concentrations the Kd increases, which means that, for the same particle flux, more ^{230}Th is scavenged so that $^{230}Th_{diss}$ decreases, and the flux to the sediment increases slightly. To test the sensitivity of the model to such an increase of the particle settling rate we conducted the "Sinking Velocity" run with the particle settling rate increased to 6 m/d. This halved the particle concentration in the water column, thereby significantly worsening the fit to observations. It also caused the fit of the model to the

observed water-column profiles of ^{230}Th concentration to degrade significantly (Fig. 3c). But the pattern and magnitude of ^{230}Th flux to sediment was still close to that seen for the 3 m/d "Holocene" run (Figs. 6a and c). In other words, the water-column distribution of ^{230}Th is more sensitive to changes in the particle settling rate than is the ^{230}Th flux to sediment. As the "Holocene" model provides a reasonable replication of the water-column data, this give us additional confidence in the robustness of the ^{230}Th flux map.

There are two aspects of particle settling that are not replicated by the model. The first of these is seasonal variability. The effects of seasonal variability can be significant for the shorter-lived Th isotopes but, for ^{230}Th, are not expected to be important. The annual production of ^{230}Th is ≈ 0.02 dpm/1000 l, so, at steady state, only seawater with < 0.2 dpm/1000 l will exhibit an annual cycle in dissolved or total ^{230}Th concentration of $> 10\%$, even if all the ^{230}Th is removed in a single annual pulse. The average seawater ^{230}Th concentration is ≈ 0.5 dpm/1000 l, so the maximum seasonal cycle is generally much smaller than this. Seasonal variation may still become significant in shallow waters, where the ^{230}Th concentrations are low, but this feature cannot be replicated by our annually resolving model and is not expected to make a difference to the annual flux of ^{230}Th to the seafloor.

The second aspect of particle settling not parametrized is spatial variability in the settling rate. In productive areas, the higher particle concentration may increase the rate of particle aggregation and therefore the rate of particle settling. The effect of this process on ^{230}Th scavenging is not easy to predict. It may result in a lowered ^{230}Th water-column inventory in highly productive regions and, in turn, cause slightly higher fluxes of ^{230}Th to the sediment in these areas. On the other hand, Colley et al. (1995) report that, for a time-series of sediment-trap data in the NE Atlantic, a linear relationship between ^{230}Th flux and mass flux breaks down during blooms when the particle flux is very high. To explain this they suggest that the high productivity results in a higher proportion of large rapidly sinking particles, which do not fully equilibrate with the dissolved ^{230}Th. At present, the relationship between particle flux and settling rate is sufficiently poorly constrained, and the effect such a relationship might have on ^{230}Th removal not well enough understood, that these effects cannot be well parametrized. It is possible that they would cause an additional focusing of ^{230}Th flux into productive regions, but we anticipate that this is unlikely to be large.

The second sensitivity test, that conducted in the "Kd value" model run, was performed by changing the Kd to particle-concentration relationship from $7.0 - 0.42.\log_{10}$(part.mass) as used in the "Holocene" and "Glacial" run, to $7.2 - 0.42.\log_{10}$(part.mass) as reported by Honeyman et al., 1988 (see Fig. 1). In this run, $^{230}Th_{diss}$ values in the water column were seen to deteriorate by a similar degree as those in the "Sinking Velocity" run (Fig. 3d), while $^{230}Th_{part.}$ values deteriorated by a lesser amount. As with the "Sinking Velocity" run, however, the normalised ^{230}Th flux to the sediment is very similar to that for the "Holocene" run, suggesting that small changes in the Kd value do not alter the principal conclusions of this study. The high sensitivity of the water-column values to changes in Kd, however, demonstrate that it is important to constrain this variable as accurately as possible in order to model ^{230}Th values in the water column.

4.5. ^{230}Th flux to sediment versus surface productivity

The ^{230}Th flux-to-sediment maps demonstrate that ^{230}Th removal is closely linked to surface productivity (Fig. 6). This gives rise to the possibility that a general relationship between productivity and ^{230}Th flux could be derived, which might be used to more carefully evaluate the use of ^{230}Th values to calculate sedimentary fluxes. Fig. 7 shows the normalised ^{230}Th flux-to-sediment for the Holocene (and also for the Glacial) plotted against the flux of POC out of the surface layer for each ice-free grid point of the model. At POC fluxes of less than about 20 gC/m^{2}a, the normalised flux is less than 1.0 while, as POC production increase to values higher than this, the ^{230}Th normalised flux is > 1.0 but tends to flatten off at values of ≈ 1.2 at very high POC productivities. This relationship therefore has a form somewhat similar to the trap data of Colley et al. (1995), in which higher particle fluxes initially increased the ^{230}Th flux but, as particle fluxes increased further, the ^{230}Th flux levelled off.

The model results shown in Fig. 7, however, also demonstrate the problems of attempting to derive a general relationship between productivity and ^{230}Th flux. The flux of ^{230}Th is controlled not just by the productivity at the location of interest, but also by the productivity upstream of this location, and by the rate of advection of water into the location. This is demonstrated by the high scatter of ^{230}Th fluxes at POC productivities of between 40 and 80 gC/m^2/a. Some productive areas are downstream of productive areas, while others are downstream of less productive regions and therefore have more ^{230}Th advected into them to be scavenged. Although the relationship shown in Fig. 7 gives some idea of the ^{230}Th flux to the sediment, the scatter about this relationship demonstrates that it is necessary to look at the particular site of interest in order to gain a full understanding of the flux of ^{230}Th to sediment at that location.

5. "Glacial" model results

As ^{230}Th profiling is widely used not just in the Holocene, but also through glacial periods, it is important to constrain the ^{230}Th flux to sediment during these periods as well. To do this we have used the velocity field of the Hamburg LSG-OGCM run with LGM boundary conditions (CLIMAP, 1981; Winguth et al., 1996) as input for the HAMOCC model and the Th model. The LGM version of the LSG-OGCM model uses wind-stress derived from an atmospheric GCM and salinity from planktonic foraminiferal δ^{18}O values to force the circulation and achieves a reasonable fit to the glacial δ^{13}C distribution as recorded in foraminifera. The model's deep-water formation is sensitive to the salinity fields used but gives a best-guess NADW that is slightly shallower than that of the Holocene model and is reduced by about 50% in volume. The glacial productivity is some 10% higher than the Holocene model, and ice cover is larger, yielding a change in sea-ice extent that is comparable to the CLIMAP reconstruction of the glacial.

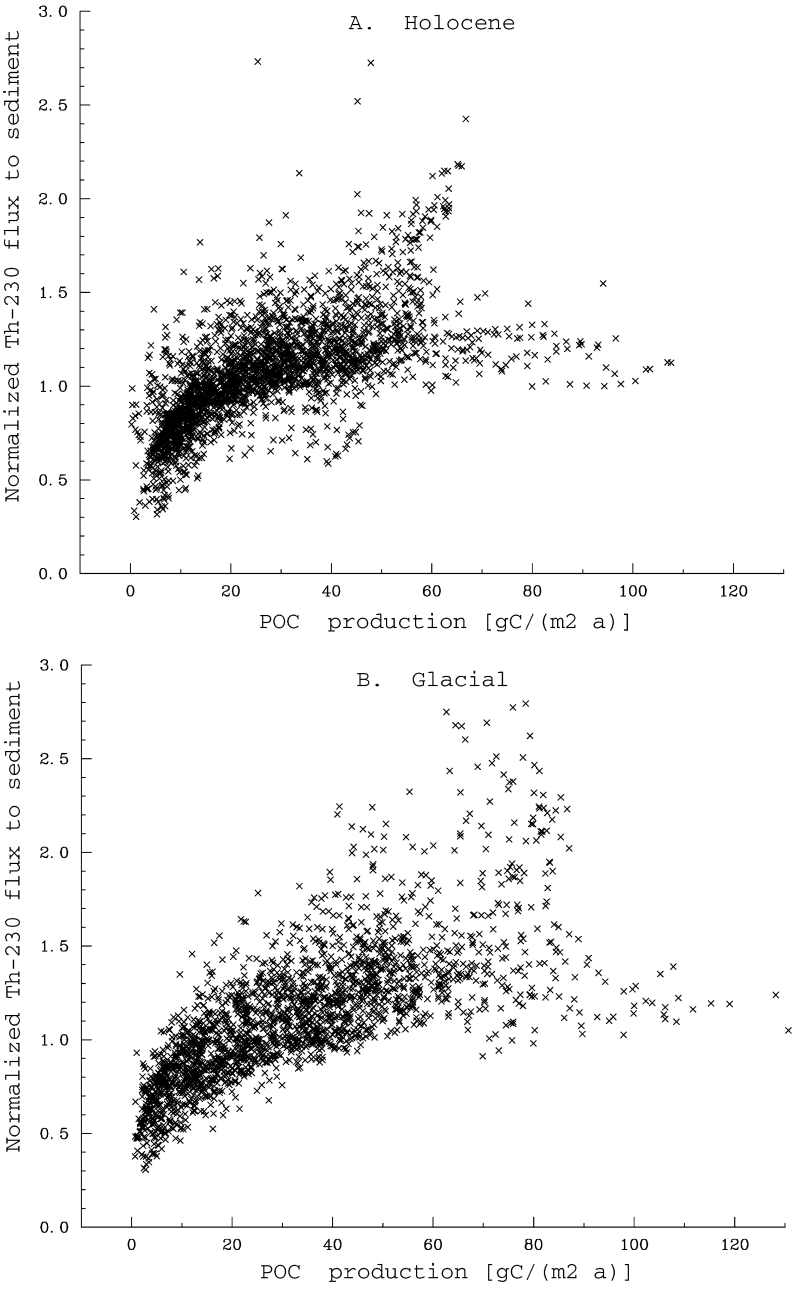

Fig. 7. Model-output normalised ^{230}Th fluxes versus POC flux out of the surface layer for ice-free grid points showing the relationship between export production and ^{230}Th flux and the degree of scatter about this relationship. (a) Holocene, and (b) Glacial.

Particle handling was added in the same way as for the Holocene run, using the same Kd relationship, the same particle settling rate and the same under-ice particle production mechanism. Model output of water column ^{230}Th profiles are shown in Fig. 3b against the modern observed values; of the western Atlantic ^{230}Th section in Fig. 5b; and of the ^{230}Th flux to sediment in Fig. 6b. Additionally, a difference map of the Glacial minus Holocene normalised ^{230}Th flux is given in Fig. 6e. This work represents the first assessment of the advection and scavenging of ^{230}Th in the glacial ocean. While these results are inevitably less robust than those for the "Holocene" run, they provide an indication of the possible differences between ^{230}Th behaviour in these two time intervals.

Several differences are seen in the "Glacial" case compared to the "Holocene". The most significant of these is due to the extended sea ice during glacial periods. As little scavenging occurs under the ice, significant amounts of ^{230}Th are advected from under the larger expanse of sea ice to be scavenged close to their margins. This leads to higher fluxes of ^{230}Th to sediment in the North Pacific, North Atlantic, and Southern Ocean. The effect is most marked in the North Atlantic, where much of the Arctic Ocean acts as a source of ^{230}Th as there is no ice-free area in this basin during the glacial. In the North Atlantic, this effect is exacerbated by reduction of deep-water formation during the glacials. The normalised ^{230}Th flux just south of the sea-ice in the glacial North Atlantic is therefore higher than that seen anywhere in the Holocene ocean at 1.7. These effects are also manifested in the water column of the Labrador Sea, which has much higher ^{230}Th concentrations in the glacial. Elsewhere in the Atlantic, the lower deep-water volume leads to a more uniform flux of ^{230}Th than in the Holocene case.

This pattern of ^{230}Th removal suggests that the use of ^{230}Th normalisation in glacial sediments must be performed with care for high-latitude areas where ice effects are important. In these regions the ^{230}Th flux-to-production ratio ranges from 0.4 to 1.7 and could therefore lead to normalised sedimentation rates in error by a factor of two. The area of ocean which falls within 30% of production is also smaller for the "Glacial" run than for the "Holocene", due to the extension of sea ice. For this 58% of the ocean, however, the Glacial to Holocene change of flux is small, suggesting that for much of the ocean the ^{230}Th normalisation method for assessing changes in rain rates of sedimentary constituents is a robust tool.

6. Conclusions

By making reasonably simple additions to existing GCMs, we have duplicated observed particle concentrations and ^{230}Th distributions for the world's oceans (except the far Southern Ocean). These models support the idea that significant advection of ^{230}Th occurs, particularly in the North Atlantic and the Arctic oceans. They also provide the first maps of the deviations in ^{230}Th flux to the sediment from that expected in a zero advection case. In general, ^{230}Th fluxes are higher in productive regions and low in gyre regions or under ice. During the Holocene, the range of ^{230}Th fluxes (normalised to production in the water column) is from 0.4

to 1.4. Low values are seen in the Western North Atlantic due to rapid advection of deep water from this basin, as well as in the South Pacific gyre and in the Arctic. High values are in productive regions, particularly the Southern Ocean. In the Glacial, increased sea-ice means that fluxes are very low in the Arctic and that ^{230}Th is advected from this basin to dramatically increase the flux to the sediment in the North Atlantic. Elsewhere in the Atlantic, normalised fluxes are more uniform than in the Holocene due to the decreased NADW production. Advection of ^{230}Th from under ice also increases ^{230}Th fluxes in the Southern Ocean and North Pacific. The glacial range of normalised ^{230}Th fluxes is 0.4–1.7. These results suggest that, at least in some areas, care should be taken in using ^{230}Th to normalise sedimentary fluxes of other species. The maps presented here, however, allow assessment of the direction of error in using this technique for any region, and of the approximate magnitude of this error. They indicate that 60–70% of the ocean is expected to have a ^{230}Th flux staying within 30% of water column production. In these areas, the use of ^{230}Th profiling is therefore expected to be a robust tool.

Acknowledgements

Michiel Rutgers van der Loeff and an anonymous reviewer are thanked for their constructive reviews. This work was supported by the US National Science Foundation (grant OPP 95 30379) as part of the US Joint Global Ocean Flux Study and is US JGOFS contribution no. 452. This is LDEO contribution No. 5943.

References

Anderson, R.F., Bacon, M.P., Brewer, P.G., 1983a. Removal of ^{230}Th and ^{231}Pa at ocean margins. Earth and Planetary Science Letters 66, 73–90.

Anderson, R.F., Bacon, M.P., Brewer, P.G., 1983b. Removal of ^{230}Th and ^{231}Pa from the open ocean. Earth and Planetary Science Letters 62, 7–23.

Anderson, R.F., Fleisher, M.Q., Biscaye, P.E., Kumar, N., Dittrich, B., Kubik, P., Suter, M., 1994. Anomalous boundary scavenging in the Middle Atlantic Bight: evidence from ^{230}Th , ^{231}Pa , ^{10}Be and ^{210}Pb. Deep-Sea Research II 41 (2/3), 537–561.

Bacon, M.P., Anderson, R.F., 1982. Distribution of thorium isotopes between dissolved and particulate forms in the deep ocean. Journal of Geophysical Research 87 (C3), 2045–2056.

Bacon, M.P., Rutgers van der Loeff, M.M., 1989. Removal of thorium-234 by scavenging in the bottom nepheloid layer of the ocean. Earth Planetary Science Letters 92, 157–164.

Bacon, M.P., Huh, C.-A., Fleer, A.P., Deuser, W.G., 1985. Seasonality in the flux of natural radionuclides and plutonium in the deep Sargasso Sea. Deep-Sea Research 32 (3), 273–286.

Bacon, M.P., Huh, C.-A., Moore, R.M., 1989. Vertical profiles of some natural radionuclides over the Alpha ridge, Arctic Ocean. Earth and Planetary Science Letters 95, 15–20.

Bacon, M.P., Rosholt, J.N., 1982. Accumulation rates of Th-230, Pa-231, and some transition metals on the Bermuda Rise. Geochimica et Cosmochimica Acta 46, 651–666.

Biscaye, P.E., Eittreim, S.L., 1977. Suspended particulate loads and transports in the nepheloid layer of the abyssal Atlantic ocean. Marine Geology 23, 155–172.

Brewer, P.G., Nozaki, Y., Spencer, D.W., Fleer, A.P., 1980. Sediment trap experiments in the deep North Atlantic: isotopic and elemental fluxes. Journal of Marine Research 38 (4), 703–728.

Brewer, P.G., Spencer, D.W., Biscaye, P.E., Hanley, A., Sachs, P.L., Smith, C.L., Kadar, S., Fredericks, J., 1976. The distribution of particulate matter in the Atlantic ocean. Earth and planetary Science Letters 32, 393–402.

Chen, J.H., Edwards, R.L., Wasserburg, G.J., 1986. ^{238}U–^{234}U–^{232}Th in seawater. Earth and Planetary Science Letters 80, 241–251.

Clegg, S.L., Bacon, M.P., Whitfield, M., 1991. Application of a generalised scavenging model to thorium isotope and particle data at equatorial and high-latitude sites in the Pacific Ocean. Journal of Geophysical Research 96(C11), 20,655-20,670.

Clegg, S.L., Whitfield, M., 1991. A generalized model for the scavenging of trace metals in the open ocean - II. Thorium scavenging. Deep-Sea Research 38 (1), 91–120.

Clegg, S.L., Whitfield, M., 1993. Application of a generalized scavenging model to time series ^{234}Th and particle data during the JGOFS North Atlantic bloom experiment. Deep-Sea Research I 40 (8), 1529–1545.

CLIMAP. 1981. Seasonal reconstruction of the earth's surface at the last glacial maximum. Geological Society of America Map Chart Ser. MC-36.

Cochran, J.K., Buesseler, K.O., Bacon, M.P., Livingston, H.D., 1993. Thorium isotopes as indicators of particle dynamics in the upper ocean: results from the JGOFS North Atlantic Bloom experiment. Deep-Sea Research II 40 (8), 1569–1595.

Cochran, J.K., Hirschberg, D.J., Livingston, H.D., Buesseler, K.O., Key, R.M., 1995. Natural and anthropogenic radionuclide distributions in the Nansen Basin, Arctic Ocean: Scavenging rates and circulation timescales. Deep-Sea Reseach II 42 (6), 1495–1517.

Cochran, J.K., Livingston, H.D., Hirschberg, D.J., Surprenant, L.D., 1987. Natural and anthropogenic radionuclide distributions in the northwest Atlantic Ocean. Earth and Planetary Science Letters 84, 135–152.

Colley, S., Thomsom, J., Newton, P.P., 1995. Detailed ^{230}Th , ^{232}Th and ^{210}Pb fluxes recorded by the 1989/90 BOFS sediment trap time-series at 48°N, 20°W. Deep-Sea Research I 42 (6), 833–848.

Francois, R., Bacon, M.P., Suman, D.O., 1990. Thorium 230 profiling in deep-sea sediments: high resolution records of flux and dissolution of carbonate in the equatorial Atlantic during the last 24,000 years. Paleoceanography 5 (5), 761–787.

Guo, L., Santschi, P.H., Baskaran, M., Zindler, A., 1995. Distribution of dissolved and particulate ^{230}Th and ^{232}Th in seawater from the Gulf of Mexico and off Cape Hatteras as measured by SIMS. Earth and Planetary Science Letters 133, 117–128.

Heinze, C., Maier-Reimer, E., Winguth, A.M.E., Archer, D. 1999. A global oceanic sediment model for long-term climate studies. Global Biogeochemical Cycles, 13 (1), 221–250.

Heinze, C., Maier-Reimer, E., Winn, K., 1991. Glacial pCO_2 reduction by the world ocean: Experiments with the Hamburg carbon cycle model. Paleoceanography 6, 395–430.

Hoff, J.A., Edwards, R.L., Buesseler, K.O., Belastock, R.A. (press) TIMS measurements of ^{230}Th and ^{232}Th in liter-sized samples of seawater from the Northwest Atlantic Ocean. Geochimica et Cosmochimica Acta.

Honeyman, B.D., Balistrieri, L.S., Murray, J.W., 1988. Oceanic trace metal scavenging: the importance of particle concentration. Deep-Sea Research 35 (2), 227–246.

Huh, C.-A., Beasley, T.M., 1987. Profiles of dissolved and particulate thorium isotopes in the water column of coastal Southern California. Earth and Planetary Science Letters 85, 1–10.

Krishnaswami, S., Lal, D., Somayajulu, B.L.K., 1976. Large-volume in-situ filtration of deep Pacific waters: Mineralogical and radioisotope studies. Earth and Planetary Science Letters 32, 420–429.

Krishnaswami, S., Sarin, M.M., Somayajulu, B.L.K., 1981. Chemical and radiochemical investigations of surface and deep particles of the Indian ocean. Earth and Planetary Science Letters 54, 81–86.

Ku, T.-L., Broecker, W.S., 1967. Rates of sedimentation in the Arctic Ocean. Progress in Oceanography 4, 95–104.

Lao, Y., Broecker, W.S., Hofmann, H.J., Wolfi, W., 1993. Particulate fluxes of ^{230}Th, ^{231}Pa, and ^{10}Be in the northeastern Pacific Ocean. Geochimica et Cosmochimica Acta 57, 205–217.

Luo, S., Ku, T.-L., Kusakabe, M., Bishop, J.K.B., Yang, Y.-L., 1995. Tracing particle cycling in the upper ocean with ^{230}Th and ^{228}Th: An investigation in the equatorial Pacific along 140°W. Deep-Sea Research II 42 (2-3), 805–829.

Maier-Reimer, E., 1993. Geochemical cycles in an ocean general circulation model. Preindustrial tracer distributions. Global Biogeochemical Cycles 7 (3), 645–677.

Maier-Reimer, E., Mikolajewiczj, U., Hasselmann, K., 1993. Mean circulation of the Hamburg LSG OGCM and its sensitivity to the thermohaline surface forcing. J. Phys. Oceanogr. 23, 731–757.

Mangini, A., Key, R.M., 1983. A ^{230}Th profile in the Atlantic ocean. Earth and Planetary Science Letters 62, 377–384.

Marcantonio, F., Kumar, N., Stute, M., Anderson, R.F., Seidl, M.A., Schlosser, P., Mix, A., 1995. A comparative study of accumulation rates derived by He and Th isotope analysis of marine sediments. Earth and Planetary Science Letters 133, 549–555.

McKee, B.A., DeMaster, D.J., Nittrouer, C.A., 1986. Temporal variability in the partitioning of thorium between dissolved and particulate phases on the Amazon shelf: implications for the scavenging of particle-reactive species. Continental Shelf Research 6, 87–106.

Moore, R.M., Hunter, K.A., 1985. Thorium adsorption in the ocean: reversibility and distribution amongst particle sizes. Geochimica et Cosmochimica Acta 49, 2253–2257.

Moore, W.S., 1981. The thorium isotope content of ocean water. Earth and Planetary Science Letters 53, 419–426.

Moran, S.B., Charett, M.A., Hoff, J.A., Edwards, R.L., Landing, W.M., 1997. Distribution of ^{230}Th in the Labrador Sea and its relation to ventilation. Earth and Planetary Science Letters 150, 151–160.

Moran, S.B., Hoff, J.A., Buesseler, K.O., Edwards, R.L., 1995. High precision ^{230}Th and ^{232}Th in the Norwegian Sea and Denmark by thermal ionization mass spectrometry. Geophysical Research Letters 22 (19), 2589–2592.

Murnane, R.J., 1994. Determination of thorium and particulate matter cycling parameters at station P: A reanalysis and comparison of least squares techniques. Journal of Geophysical Research 99 (C2), 3393–3405.

Murnane, R.J., Sarmiento, J.L., Bacon, M.P., 1990. Thorium isotopes, particle cycling models, and inverse calculations of model rate constants. Journal of Geophysical Research 95(C9), 16,195–16,206.

Najjar, R.G., Sarmiento, J.L., Toggweiler, J.R., 1992. Downward transport and fate of organic matter in the ocean: Simulations with a general circulation model. Global Biogeochemical Cycles 6, 45–76.

Nozaki, Y., Horibe, Y., 1983. Alpha-emitting thorium isotopes in northwest Pacific deep waters. Earth and Planetary Science Letters 65, 39–50.

Nozaki, Y., Horibe, Y., Tsubota, H., 1981. The water column distributions of thorium isotopes in the western North Pacific. Earth and Planetary Science Letters 54, 203–216.

Nozaki, Y., Nakanishi, T., 1985. ^{231}Pa and ^{230}Th in the open ocean water column. Deep-Sea Research 32 (10), 1209–1220.

Nozaki, Y., Yamada, M., 1987. Thorium and protactinium isotope distributions in waters of the Japan Sea. Deep-Sea Research 34 (8), 1417–1430.

Nozaki, Y., Yang, H.-S., 1987. Th and Pa isotopes in the waters of the western margin of the Pacific near Japan: Evidence for release of ^{228}Ra and ^{227}Ac from slope sediments. Journal of Oceanographic Society of Japan 43, 217–227.

Nozak, Y., Yang, H.-S., Yamada, M., 1987. Scavenging of thorium in the ocean. Journal of Geophysical Research 92 (C1), 772–778.

Roy-Barman, M., Chen, J.H., Wasserburg, G.J., 1996. ^{230}Th–^{232}Th systematics in the central Pacific Ocean The sources and the fates of thorium. Earth and Planetary Science Letters 139, 351–363.

Rutgers van der Loeff, M.M., Berger, G.W., 1993. Scavenging of ^{230}Th and ^{231}Pa near the Antarctic Polar front in the South Atlantic. Deep-Sea Research 40 (2I), 339–357.

Santschi, P.H., Honeyman, B.D., 1991. Radioisotopes as tracers for the interactions between trace elements, colloids and particles in natural waters. In: Vernet, J.-P. (Ed.), Trace Metals in the Environment 1. Heavy Metals in the Environment, Elsevier, Amsterdam, pp. 229–246.

Scholten, J.C., Rutgers, van der Loeff, M.M., Michel, A., 1995. Distribution of ^{230}Th and ^{231}Pa in the water column in relation to the ventilation of the deep Arctic basins. Deep-Sea Research II 42 (6), 1519–1531.

Suman, D.O., Bacon, M.P., 1989. Variations in Holocene sedimentation in the North American Basin determined by ^{230}Th measurements. Deep Sea Research 36, 869–887.

Taguchi, K., Harada, K., Tsunogai, S., 1989. Particulate removal of ^{230}Th and ^{231}Pa in the biologically productive northern North Pacific. Earth and Planetary Science Letters 93, 223–232.

Thomson, J., Colley, J., Anderson, R., Cook, G.T., MacKenzie, A.B., 1997. A comparison of sediment accumulation chronologies by radiocarbon and $^{230}Th_{xs}$ methods. Earth and Planetary Science Letters 133, 59–70.

Tsunogai, S., Minagawa, M., 1978. Settling model for the removal of insoluble chemical elements in seawater. Geochemical Journal 12, 47–56.

Vogler, S., Scholten, J., Rutgers van der Loeff, M., Mangini, A., 1998. ^{230}Th in the eastern North Atlantic: the importance of water mass ventilation in the balance of ^{230}Th. Earth and Planetary Science Letters 156, 61–74.

Vogler, S., Scholten, J., Rutgers van der Loeff, M., Mangini, A. (press) ^{230}Th and ^{232}Th in seawater determined by thermal ionization mass-spectrometry (TIMS): Implications for particle dynamics in the North Atlantic. Earth and Planetary Science Letters.

Volk, T., Hoffert, M., 1985. Ocean carbon pumps: Analysis of relative strengths and efficiencies in ocean-driven pCO_2 changes. In: Sundquist, E.T., Broecker, W.S., (Eds.), The Carbon Cycle and Atmospheric CO_2: Natural Variations Archean to Present, Geophysical Monograph Series, Vol. 32, pp. 99–110, Washington DC.

Walter, H.J., Rutgers van der Loeff, M.M., Hoeltzen, H., 1997. Enhanced scavenging of ^{231}Pa relative to ^{230}Th in the South Atlantic south of the Polar front: implications for the use of the ^{231}Pa/^{230}Th ratio as a paleoproductivity proxy. Earth and Planetary Science Letters 149, 85–100.

Winguth, A.M.E., Maier-Reimer, E., Mikolajewicz, U., Duplessy, J.-C. 1996. On the sensitivity of an ocean general circulation model to glacial boundary conditions. Max Plank Institut fur Meteorologie.

Yu, E.F., 1994. Variations in the particulate flux of ^{230}Th and ^{231}Pa and paleoceanographic applications of the ^{231}Pa/^{230}Th ratio. Ph. D., Thesis, MIT/WHOI, WHOI-94–21.